

Skyra: AI-Generated Video Detection via Grounded Artifact Reasoning

Yifei Li, Wenzhao Zhen[†], Yanran Zhang, Runze Sun, Yu Zheng, Lei Chen, Jie Zhou, Jiwen Lu*
 Department of Automation, Tsinghua University
 Project Page: <https://joeleelyf.github.io/Skyra>

Abstract

The misuse of AI-driven video generation technologies has raised serious social concerns, highlighting the urgent need for reliable AI-generated video detectors. However, most existing methods are limited to binary classification and lack the necessary explanations for human interpretation. In this paper, we present **Skyra**, a specialized multimodal large language model (MLLM) that identifies human-perceivable visual artifacts in AI-generated videos and leverages them as grounded evidence for both detection and explanation. To support this objective, we construct **ViF-CoT-4K** for Supervised Fine-Tuning (SFT), which represents the first large-scale AI-generated video artifact dataset with fine-grained human annotations. We then develop a two-stage training strategy that systematically enhances our model’s spatio-temporal artifact perception, explanation capability, and detection accuracy. To comprehensively evaluate Skyra, we introduce **ViF-Bench**, a benchmark comprising 3K high-quality samples generated by over ten state-of-the-art video generators. Extensive experiments demonstrate that Skyra surpasses existing methods across multiple benchmarks, while our evaluation yields valuable insights for advancing explainable AI-generated video detection. Our code, models, and datasets are publicly available at <https://joeleelyf.github.io/Skyra>.

1. Introduction

With the rapid evolution of diffusion-based [3, 32, 50, 66, 80] and multimodal generative models [12, 31, 47], synthetic videos now achieve unprecedented levels of authenticity, enabling anyone to produce photorealistic content from simple text prompts or reference images. While this progress reshapes entertainment, communication, and design, its misuse poses growing threats to social safety [57, 76].

Driven by this urgent need, the community has developed several detection models [1, 5, 26, 49, 84, 90],

[†] Project leader.

* Corresponding author.

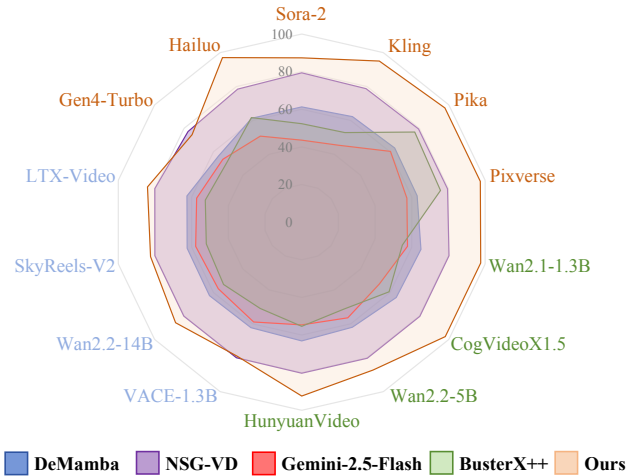


Figure 1. Performance on ViF-Bench. Our method outperforms both binary and existing MLLM-based detectors.

datasets [5, 7], and benchmarks [5, 7, 44] to detect AI-generated videos. The rise of multimodal large language models (MLLMs) [2, 25, 34, 38, 53] has attracted the attention of AI-generated content detection researchers due to their capacity for interpretable reasoning [8, 20, 37, 63, 87]. Still, we empirically find that even state-of-the-art (SoTA) general MLLM [2, 11, 48] achieves near-random performance in identifying AI-generated videos, and fails to capture human-perceivable artifacts, even with carefully designed chain-of-thought (CoT) [71] prompts. While recent works such as BusterX++ [72, 73] attempt to adapt pre-trained MLLMs for AI-generated video detection, the resulting model acts more as general content descriptors and overemphasizes superficial cues (e.g., visual quality, lighting) while neglecting the intrinsic, physics-violating artifacts that humans rely on to identify AI-generated videos (Figure 2). DAVID-XR1 [16] advancing the field by introducing human annotations of AI-generated video artifacts. However, the classification taxonomy of their annotations is vague, with the number of valid samples being limited, and the resulting model’s performance far from satisfactory.

To overcome these limitations, we introduce **Skyra**, a specialized multimodal large language model AI-generated video detection via grounded artifact reasoning, which

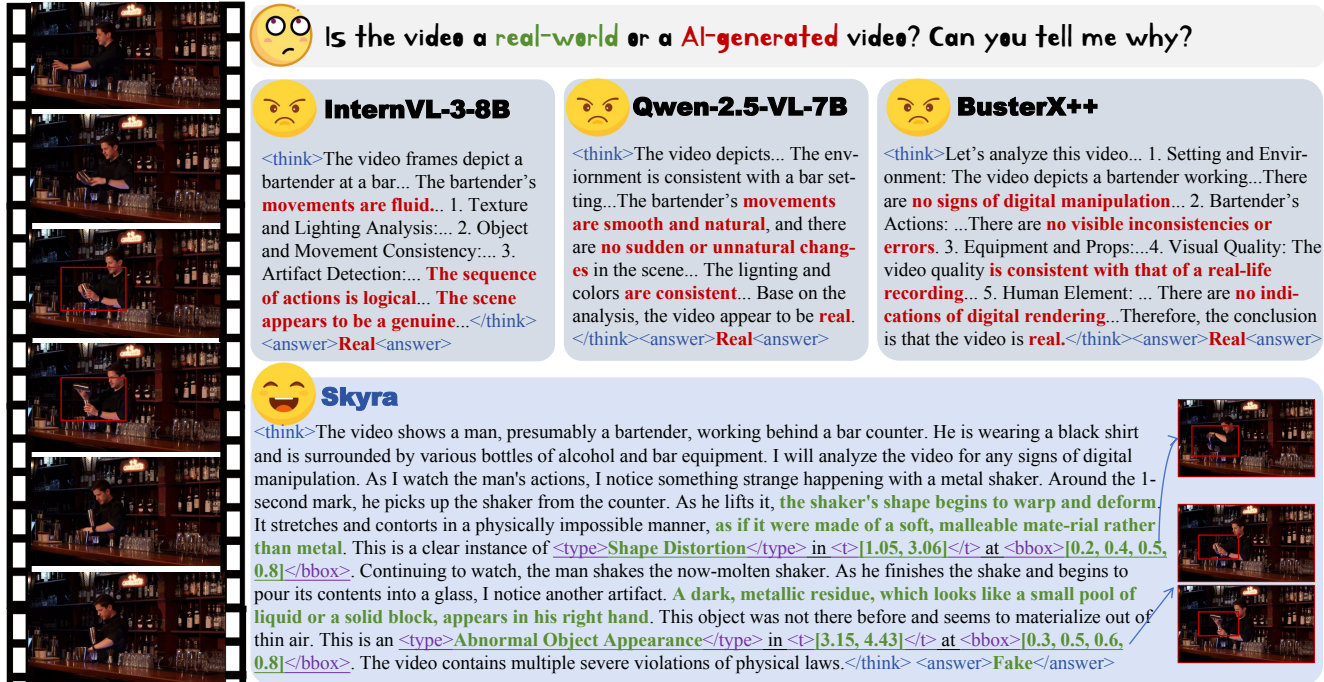


Figure 2. **Skyra** leverages human-perceivable artifacts in AI-generated videos as grounded evidence for detection and explanation. Compared to off-the-shelf MLLMs and previous MLLM-based detectors, **Skyra** demonstrates superior artifact perception and detection capabilities.

identifies artifacts and leverages them as spatio-temporally grounded evidence. As shown in Figures 1 and 2, **Skyra** achieves substantially higher detection accuracy while providing fine-grained, human-interpretable artifact localization, consistently outperforming both binary classifiers and prior MLLM-based approaches. Recognizing that off-the-shelf MLLMs lack sensitivity to subtle generative artifacts, we construct the first large-scale human-annotated AI-generated video artifacts dataset, **ViF-CoT-4K**, which enables supervised fine-tuning and yields **Skyra-SFT**. We further propose a second-stage reinforcement learning procedure that pushes forward the model’s ability to mine discriminative artifacts, producing additional gains in both detection and explanation quality, resulting in our final model **Skyra-RL**. To comprehensively evaluate the ability of existing methods, we release **ViF-Bench**, which includes high-quality samples generated by over ten latest models, with real and fake samples aligned in both semantics and formats, mitigating shortcut signals, and providing a fair testbed of artifact-based detection.

2. Related Work

AI-Generated Video Detection. AI-generated video detection has largely focused on binary classification [1, 5, 7, 26, 40], relying on visual artifact detection in synthetic content. Early methods like AIGVDet [1] and DeCoF [40] exploit spatio-temporal features and frame consistency to detect discrepancies, achieving strong performance on curated datasets such as GVD [1] and GVF [40]. Recent works, including DeMamba [5], D3 [90], ReStraV [26], and NSG-

VD [84], explore more discriminative and robust feature spaces, demonstrating success on updated benchmarks like GenVideo [5] and GenVidBench [44]. However, these approaches lack interpretability, leaving the detection process opaque and limiting their applicability in scenarios that require manual verification.

The emergence of MLLMs [2, 10, 25, 38, 65, 68, 82, 83] has enabled more explainable detection [20, 49, 62, 77, 87], providing both predictions and reasoning processes. X2-DFD [8] and VERITAS [63] demonstrate MLLM effectiveness in deepfake face detection through pattern-aware reasoning and feature enhancement. MLLMs have also succeeded in AIGC image detection, with frameworks like FakeVLM [74] and LEGION [28] enabling fine-grained artifact identification, and UniGenDet [88] unifying image generation and generated-image detection within a single co-evolutionary framework. For video content, MLLM-based methods remain nascent. IVY-Fake [85], DAVID-XR1 [16], and BusterX++ [72, 73] pioneer explainable video detection, providing interpretable reasoning on motion, texture, and temporal artifacts. Concurrently, DeepTraceReward [15] studies human-perceived fakeness in AI-generated videos through multimodal LLMs, proposing evaluation metrics for explanation quality including spatial and temporal localization accuracy. Despite progress, current methods struggle with complex temporal dynamics and fine-grained reasoning, often relying on MLLM-generated annotations [65, 85] or basic fine-tuning [16, 85]. In contrast, our approach leverages high-quality human annotations and precise spatio-temporal

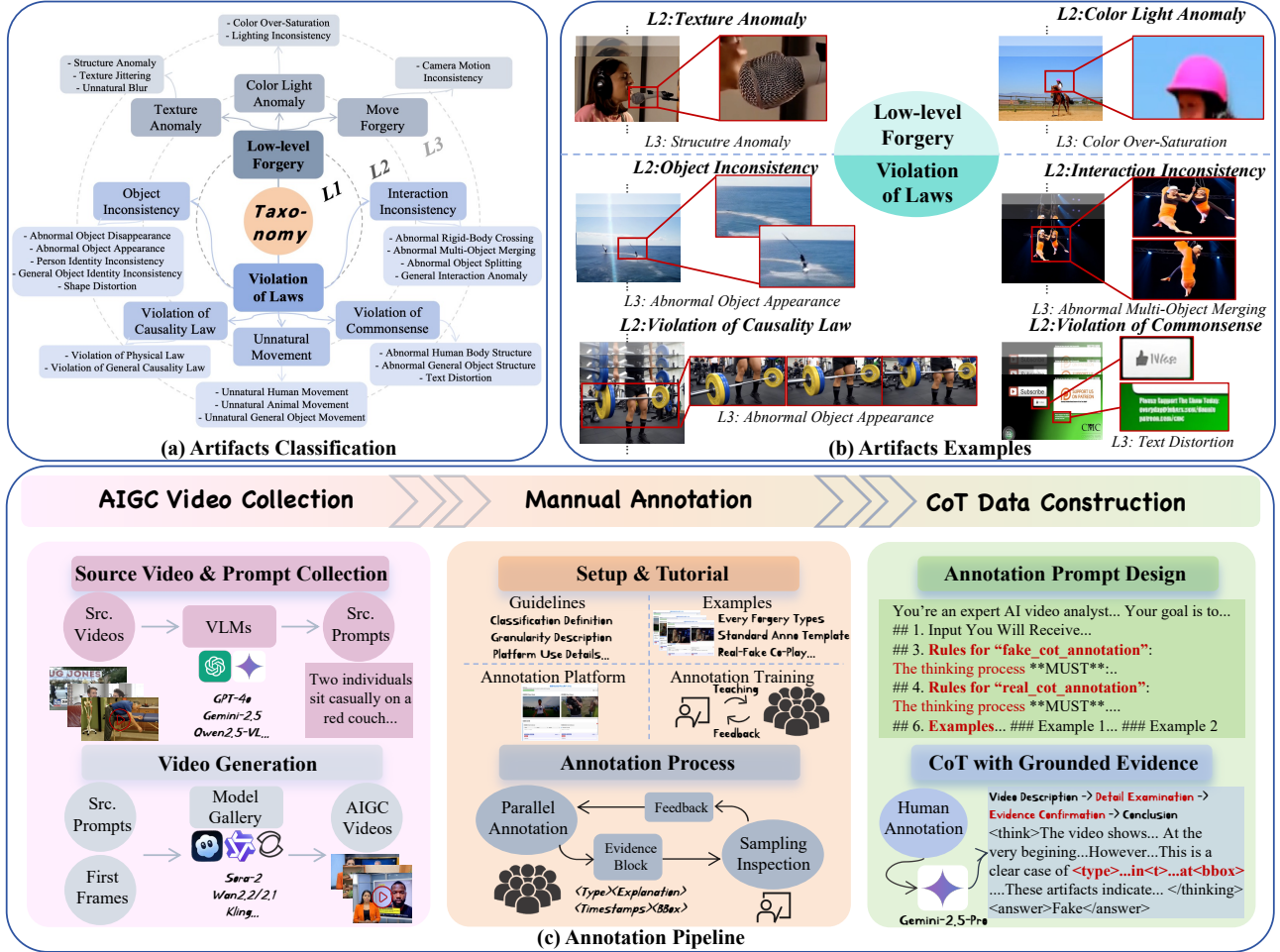


Figure 3. Overview of the ViF-CoT-4K dataset. (a) The hierarchical taxonomy of AI-generated video artifacts. (b) Visual examples of artifacts under our taxonomy. (c) Construction pipeline of ViF-CoT-4K dataset, including authentic data collection and AI-generated video collection, manual annotation, and the step-by-step chain-of-thought explanation data construction process.

supervision to enhance artifact perception and reasoning.

Multimodal Large Language Models for Video. Recent advances in video MLLMs have yielded specialized architectures for video processing and reasoning. VideoChatGPT [41] integrates a video-adapted visual encoder with an LLM for detailed understanding through conversation. Video-LLaMA [82] employs multimodal encoders for spatio-temporal reasoning, integrating audio and video for enhanced comprehension. Meanwhile, general vision-language models have also demonstrated strong video capabilities. Qwen2-VL [68] introduces dynamic-resolution tokenization and unified image-video encoding. Recent models like Seed1.5VL [17], InternVL3.5 [69], and Qwen3VL [53] further advance visual-temporal feature integration, achieving strong performance on diverse benchmarks [35, 45, 70, 75].

Despite these advances, base MLLMs exhibit limited reasoning without task-specific fine-tuning. Post-training strategies, particularly reinforcement learning (RL) [61, 64], have emerged to address this gap. In the image domain,

OpenThinkIMG [60] and DeepEyes [91] incorporate RL to enhance visual reasoning through structured, multi-stage processes. For video understanding, Video-R1 [13] introduces T-GRPO for temporally consistent reasoning, while LongVILA-R1 [9] integrates RL with large-scale reasoning tasks to support longer inputs. Recent methods [14, 22, 79] enhance reasoning by incorporating tool use into trajectories, achieving state-of-the-art performance. These RL-based strategies are essential for enhancing MLLMs' perception [33, 39, 86] and reasoning [19, 24, 89], particularly for challenging video understanding tasks [64].

3. ViF Dataset

With rapid advances in AI video generation technologies [12, 47, 66, 80], numerous datasets [5, 7, 72] and benchmarks [5, 7, 44] have emerged for detection research. However, existing datasets face three key limitations: (1) **Significant Real-Fake Discrepancy**: In datasets like [5, 7, 44], real videos exhibit 2-3× higher duration and FPS than fake

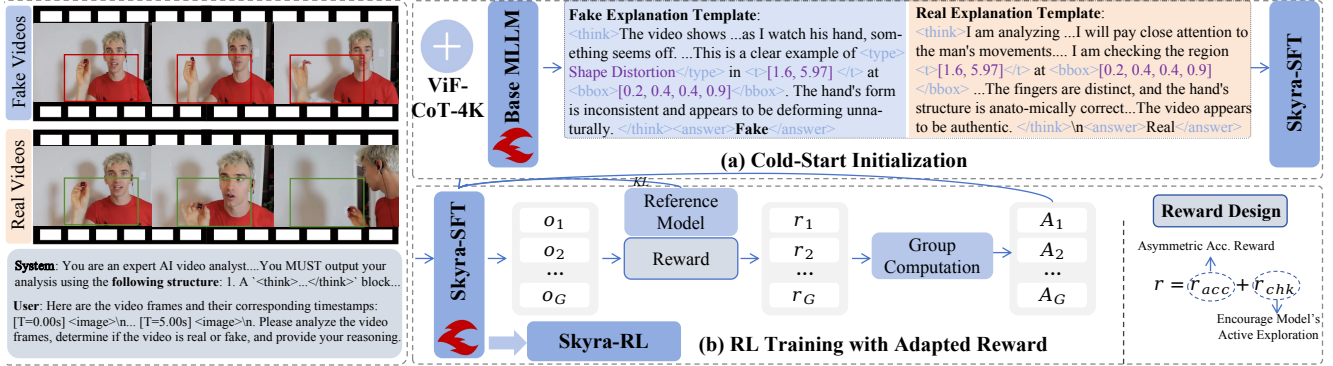


Figure 5. Overview of Skyra. We leverage a two-stage training pipeline to improve Skyra’s artifacts perception and detection capabilities: (a) cold-start initialization with balanced fake and real explanation response templates to endow the base model with basic AI-generated artifacts perception capability. (b) reinforcement learning with adapted rewards to encourage the model’s self-driven visual probe process.

mains. For training, we use Wan2.2-TI2V-5B [66], Wan2.1-T/2V-1.3B [66], CogVideoX-1.5-5B [80], and Hunyuan-Video [32]. For evaluation, we include recent models like Wan2.2-T/2V-A14B [66], LTX-Video-13B [21], MiniMax-Hailuo [43], and Sora-2 [47]. See Table 1 for details.

Fine-grained Manual Annotation. We collaborate with domain experts to develop detailed annotation guidelines and build an easy-to-use annotation platform. Professional annotators familiar with video generation models identify all visible artifacts (*fake evidence*) in AI-generated videos, annotating: (1) artifact **Type** from our taxonomy, (2) **Textual Explanation**, (3) temporal-spatial localization via **Timestamps** and **Bounding Boxes**. Notably, we display AI-generated videos alongside real counterparts, prompting annotators to identify corresponding *real evidence* in real videos for each *fake evidence*. This helps to validate that artifacts are truly generation-induced rather than compression-related degradation. Multiple review cycles ensure annotation quality and inter-annotator consistency.

Chain-of-Thought (CoT) Annotation. Chain-of-thought reasoning improves MLLM performance on complex visual tasks [71]. While precise, our manual labels lack step-by-step reasoning valuable for model training. For each AI-generated video, we feed artifact **Type**, **Textual Explanation**, **Timestamps**, and **Bounding Boxes** aligned with sampled frames to Gemini-2.5-Pro [11]. For real videos, we substitute *fake evidence* with *real evidence* as model input. To improve the quality of annotation generated by Gemini-2.5-Pro, we employ two prompt-engineering strategies. (1) **Self-Curation:** we instruct the model to follow an *observe-understand-draft-review-conclude* process, grounding CoT in visual details; (2) **In-Context Learning:** we provide detailed definitions and carefully crafted CoT examples for each artifact type, filtering mismatched annotations.

4. Skyra

In this section, we analyze the characteristics of the AI-generated video detection and explanation, examine the chal-

lenges of applying off-the-shelf MLLMs to this task, and present our design motivation (Section 4.1). We then introduce our two-stage training strategies as depicted in Figure 5, i.e., supervised fine-tuning to endow the model with basic detection and explanation capabilities (Section 4.2), and reinforcement learning to enhance its ability to perceive and reason about AI-generated artifacts (Section 4.3).

4.1. Analysis of the AI-Generated Video Detection and Explanation Task

How Humans Identify AI-Generated Videos. Conventional AIGC detection approaches typically extract hand-crafted [26, 84, 90] or learned features [1, 5, 7] from generative samples and perform binary classification in this feature space. However, this paradigm often devolves into a continuous adversarial cycle between detectors and generators: as new generative models emerge, previous discriminative features may lose effectiveness. This results in detectors that lack generalizability and remain fragile when encountering unseen samples [92].

To move beyond this limitation, we examine how humans identify AI-generated videos. Humans first perceive the overall semantic and temporal context, then actively search for spatio-temporal inconsistencies, such as abrupt object disappearance, unnatural motions, or implausible scene transitions that reveal synthetic content. Through continuous interaction with the real world, humans develop a grounded understanding of physical and temporal coherence [56, 58, 59], enabling intuitive recognition of violations. We refer to such cues as *intrinsic evidences*, as they are universal, model-agnostic indicators of deviation from real-world dynamics.

Challenges of Adapting MLLMs for AI-Generated Video Detection. Pre-trained on large-scale vision-language datasets, MLLMs have acquired a foundational understanding of the real world to some extent. Inspired by prior work [87], we explored directly prompting off-the-shelf MLLMs for AIGC video detection. However, both direct question-answer prompting and carefully designed chain-of-

thought (CoT) strategies yield limited accuracy, often below 60% on our benchmarks (Table. 1).

Our experimental analysis reveals two key issues: (1) most existing MLLMs [2, 48, 69, 82], even with explicit step-by-step CoT guidance, struggle to uncover subtle spatiotemporal forgery cues; and (2) some models [11] misinterpret natural video degradations (e.g., compression artifacts, motion blur) as forgery signs, leading to false positives on real videos. Detailed examples are provided in the Appendix. These observations motivate our approach to emulate human reasoning, i.e., enhancing the model ability to discover essential forgery cues while incorporating self-verification to re-examine suspected regions in real videos, improving both precision and confidence.

4.2. Cold-start Initialization

Response Template Design. We require the model to ground its judgment on careful video inspection and explicitly expose its reasoning process. This chain-of-thought (CoT) supervision is essential for improving accuracy and credibility (see Ablation-II in Section 5.3). The model follows the format F_{outer} :

```
<thinking>[thinking process]</thinking>
<answer>[Fake / Real]</answer>
```

For **fake** videos, we guide attention to forged regions using F_{fake} : `<type>[Forgery Type]</type>` in `<t>[t_start, t_end]</t>` at `<bbox>[x_min, y_min, x_max, y_max]</bbox>`.

For **real** videos, the model instead inspects suspected regions with the same temporal-spatial tags F_{real} : `<t>[t_start, t_end]</t>` at `<bbox>[x_min, y_min, x_max, y_max]</bbox>`

Training Process. We fine-tune Qwen2.5-VL-7B on our ViF-CoT-4K dataset. Text t and video v are encoded by pretrained textual and visual encoders, fused, and fed into the decoder for autoregressive generation. Given the ground-truth response sequence $y^* = (y_1^*, \dots, y_T^*)$, the model is trained with standard cross-entropy loss:

$$\mathcal{L}_{SFT} = - \sum_{t=1}^T \log p_{\theta}(y_t^* | y_{<t}^*, t, v), \quad (1)$$

where θ denotes model parameters. We show in ablation experiments (Ablation-II (Section 5.3)) that this cold-start stage is crucial for endowing the model with essential detection and explanation abilities. Without this initialization, the base model’s forgery recognition capacity remains weak, leading to sparse rewards in the subsequent RL stage and preventing effective learning of meaningful forensic cues.

4.3. RL Training

We observe that during the data annotation process, human annotators struggled to identify precise artifact cues in certain high-quality generated samples. Conversely, for low-quality samples, human-provided labels often contain signifi-

cant noise. Therefore, in this stage, we employ reinforcement learning (RL) to elicit the model’s inherent capability for self-coherent forgery cue discovery. This approach also aims to continuously improve adaptability to new domains, mitigating the need for iterative manual annotation. We adopt Group Relative Policy Optimization (GRPO) [18, 55] as our RL algorithm, where we re-design the reward score to adapt it to our task.

For each query-completion pair (x, y) , the total reward $R(x, y)$ is defined as:

$$R(x, y) = w_{acc} \cdot r_{acc}(x, y) + w_{chk} \cdot r_{chk}(x, y) \quad (2)$$

where $w_{acc} = 0.8$ and $w_{chk} = 0.2$ in our experiments. The rewards $r_{acc}(x, y)$ and $r_{chk}(x, y)$ are defined as follows:

Accuracy Reward $r_{acc}(x, y)$. We apply an asymmetric reward structure with more severe penalties for false positives:

$$r_{acc}(x, y) = \begin{cases} 1.0 & \text{if } y_{pred} = y_{gt} \\ 0.0 & \text{if } y_{gt} = \text{“Fake”} \wedge y_{pred} = \text{“Real”} \\ -0.2 & \text{if } y_{gt} = \text{“Real”} \wedge y_{pred} = \text{“Fake”} \end{cases} \quad (3)$$

Check Reward $r_{chk}(x, y)$. This reward is activated only when the model’s response adheres to the prescribed format F_{outer} . We extract the number of valid check blocks N_{check} from the model output using regular expressions. The matching pattern follows F_{fake} when the prediction is “Fake”, and F_{real} when the prediction is “Real”:

$$r_{chk}(x, y) = \min(\ln(1 + N_{check}), \ln(1 + 3)) \quad (4)$$

Our reward function encourages active cue exploration while strictly supervising the classification. We observed that symmetric penalties for both error types (false positives and false negatives) caused the model to overfit and develop a strong bias towards predicting “Fake”. This stems from the inherent asymmetry of the task, i.e., identifying “Fake” requires finding just one artifact, while confirming “Real” requires comprehensively ruling out all inconsistencies. We validate our asymmetric design in Ablation-III (Section 5.3).

5. Experiments

5.1. Experimental Setup

Implementation Details. We build upon Qwen2.5-VL-7B-Instruct popular in video-related tasks [13, 36, 42, 73], trained on 8 NVIDIA H200 GPUs. During training, we uniformly sample 16 frames from each video and resize them to 256p. In the SFT stage, we perform full-parameter fine-tuning with batch size 1 per device for 5 epochs at learning rate $1e-5$. In the RL stage, we set the actor learning rate to $5e-7$ and the KL coefficient to 0.02. For binary detectors, we use identical video pairs with fake/real labels and follow their original training protocols.

Evaluation Protocols. For binary detectors, use weights trained on our dataset and follow their preprocessing scripts. For off-the-shelf MLLMs (like GPT-4.1-mini [48]) and ours,

Table 1. Detection performances on ViF-Bench.

Method	Metric	Wan2.1	CogV	Wan2.2		Hunyuan		VACE	Wan2.2		Skyreels		LTX-Video		Gen4	Hai-	Pika	Pixverse	Kling	Sora-2	Mean
		-1.3B	-X1.5	-5B	-5B	T2V	I2V	-1.3B	T2V	T2V	I2V	T2V	I2V	-Turbo	luo-02	-V2	-V4-5	-V1	\		
Binary Detectors																					
AIGVDet	Acc	82.12	81.21	67.58	62.73	77.44	90.00	58.48	71.52	72.12	75.15	66.46	65.31	67.48	56.25	70.07	55.30	73.68	58.87	60.67	69.08
	R	70.91	69.09	41.82	32.12	61.59	96.92	23.64	49.70	50.91	56.97	39.63	37.50	41.72	17.86	43.80	15.89	53.95	21.99	26.67	44.88
	F1	79.86	78.62	56.33	46.29	73.19	90.65	36.28	63.57	64.62	69.63	54.17	51.95	56.20	28.99	59.41	26.23	67.21	34.83	40.40	56.76
DeMamba	Acc	65.45	65.76	65.76	60.00	65.85	60.30	61.82	65.76	61.82	65.76	64.02	64.06	64.11	62.50	64.23	66.89	66.78	67.02	63.67	64.29
	R	99.39	100.00	100.00	88.48	100.00	89.09	92.12	100.00	92.12	100.00	96.34	96.88	96.32	91.96	97.81	100.00	100.00	100.00	96.00	96.66
	F1	74.21	74.49	74.49	68.87	74.55	69.18	70.70	74.49	70.70	74.49	72.81	72.94	72.85	71.03	73.22	75.12	75.06	75.20	72.54	73.00
NSG-VD	Acc	50.00	49.39	50.30	49.70	50.30	49.70	50.00	50.00	49.39	49.70	49.09	49.06	50.00	50.45	50.36	48.34	48.68	49.29	49.67	49.65
	R	99.39	98.18	100.00	98.79	100.00	98.79	99.39	99.39	98.18	98.79	97.56	97.50	99.39	100.00	100.00	96.03	96.71	97.87	98.67	98.66
	F1	66.53	65.99	66.80	66.26	66.80	66.26	66.53	66.53	65.99	66.26	65.71	65.68	66.53	66.87	66.83	65.02	65.33	65.87	66.22	66.21
Open-source Multimodal Large Language Models																					
Video-LLaMa-3(7B)	Acc	50.92	53.68	51.84	51.23	50.62	51.53	52.45	50.00	50.31	50.31	50.00	50.31	52.45	50.90	50.37	49.67	49.67	50.00	51.01	50.91
	R	2.45	7.98	4.29	3.07	1.85	3.68	5.52	0.61	1.23	1.23	0.62	1.25	5.52	2.70	0.74	0.00	0.00	0.71	2.03	2.39
	F1	4.76	14.69	8.19	5.92	3.61	7.06	10.40	1.21	2.41	2.41	1.22	2.45	10.40	5.22	1.46	0.00	0.00	1.41	3.97	4.57
Qwen-2.5-VL(3B)	Acc	52.12	54.85	50.61	50.00	50.00	50.00	50.91	50.61	50.91	50.00	49.7	52.5	49.69	50.00	50.36	50.99	50.33	49.65	50.00	50.7
	R	5.45	10.91	2.42	1.21	1.22	1.54	3.03	2.42	3.03	1.21	0.61	6.25	0.61	1.79	1.46	3.31	1.97	0.00	1.33	2.62
	F1	10.23	19.46	4.68	2.37	2.38	2.99	5.81	4.68	5.81	2.37	1.20	11.63	1.20	3.45	2.86	6.33	3.82	0.00	2.60	4.94
Qwen-2.5-VL(7B)	Acc	51.21	50.3	49.7	51.21	51.22	51.21	50.91	50.3	50.61	49.39	50.00	50.62	51.53	50.00	50.00	50.99	50.00	49.65	52.00	50.57
	R	4.85	3.03	1.82	4.85	4.88	4.85	4.24	3.03	3.64	1.21	2.44	3.75	5.52	2.68	2.19	3.97	2.63	1.42	6.00	3.53
	F1	9.04	5.75	3.49	9.04	9.09	9.04	7.95	5.75	6.86	2.34	4.65	7.06	10.23	5.08	4.20	7.50	5.00	2.74	11.11	6.63
Qwen-2.5-VL(72B)	Acc	52.42	51.82	50.91	50.3	50.61	51.52	54.55	51.21	49.39	50.00	50.30	53.12	52.45	50.00	51.82	53.31	51.97	48.58	49.67	51.26
	R	9.09	7.88	6.06	4.85	5.49	7.27	13.33	6.67	3.03	4.24	4.88	10.62	9.20	6.25	8.76	10.60	8.55	2.13	4.00	6.99
	F1	16.04	14.05	10.99	8.89	10.00	13.04	22.68	12.02	5.65	7.82	8.94	18.48	16.22	11.11	15.38	18.50	15.12	3.97	7.36	12.44
InternVL-3(8B)	Acc	48.16	57.98	46.01	48.77	50.00	50.61	55.83	45.71	46.01	45.40	46.60	50.62	49.69	45.95	47.06	50.00	48.00	44.29	46.28	48.58
	R	13.50	33.13	9.20	14.72	17.28	18.40	28.83	8.59	9.20	7.98	10.49	18.12	16.56	11.71	10.29	17.33	11.33	5.71	9.46	14.31
	F1	20.66	44.08	14.56	22.33	25.69	27.15	39.50	13.66	14.56	12.75	16.43	26.85	24.77	17.81	16.28	25.74	17.89	9.30	14.97	21.31
Proprietary Multimodal Large Language Models																					
GPT-4.1-mini	Acc	55.83	59.82	53.37	57.06	55.25	54.60	54.60	53.68	53.68	51.23	54.94	54.69	55.83	53.60	50.00	54.33	55.33	50.71	48.99	54.08
	R	18.40	26.38	13.50	20.86	17.28	15.95	15.95	14.11	14.11	9.20	16.67	16.25	18.40	12.61	8.09	16.00	16.67	8.57	4.05	14.90
	F1	29.41	39.63	22.45	32.69	27.86	26.00	26.00	23.35	23.35	15.87	27.00	26.40	29.41	21.37	13.92	25.95	27.17	14.81	7.36	24.21
Gemini-2.5-flash	Acc	57.67	52.76	57.67	55.21	55.56	50.92	58.90	49.08	49.39	53.07	46.30	57.19	59.20	53.60	50.74	60.33	57.33	45.36	43.58	53.36
	R	72.39	62.58	72.39	67.48	67.90	58.90	74.85	55.21	55.83	63.19	49.38	70.62	75.46	65.77	58.09	78.67	70.67	47.14	45.27	63.78
	F1	63.10	56.98	63.10	60.11	60.44	54.55	64.55	52.02	52.45	57.38	47.90	62.26	64.91	58.63	54.11	66.48	62.35	46.32	44.52	57.48
MLLM-based Detectors																					
BusterX++(7B)	Acc	54.85	59.39	52.42	50.30	59.15	49.70	50.91	62.42	49.70	65.76	50.00	56.25	50.00	50.89	61.68	76.82	75.66	52.84	52.33	56.90
	R	10.30	19.39	5.45	1.21	18.90	0.00	2.42	25.45	0.00	32.12	0.61	13.12	0.61	2.68	24.09	54.30	51.97	5.67	5.33	14.40
	F1	18.58	32.32	10.29	2.38	31.63	0.00	4.71	40.38	0.00	48.40	1.20	23.08	1.21	5.17	38.60	70.09	68.10	10.74	10.06	21.94
Ours-SFT(7B)	Acc	97.58	97.58	90.30	84.24	93.9	92.12	79.09	96.67	83.03	95.15	76.83	96.25	80.67	74.55	97.08	97.35	97.37	95.04	87.33	90.11
	R	99.39	99.39	84.85	72.73	92.07	88.48	62.42	97.58	70.3	94.55	57.93	96.88	65.64	54.46	98.54	99.34	99.34	95.04	79.33	84.65
	F1	97.62	97.62	89.74	82.19	93.79	91.82	74.91	96.7	80.56	95.12	71.43	96.27	77.26	68.16	97.12	97.4	97.42	95.04	86.23	88.76
Ours-RL(7B)	Acc	96.97	96.36	92.12	87.58	94.82	93.64	79.09	96.36	84.55	95.76	78.96	95.94	83.74	79.46	95.99	96.36	96.05	94.68	91.00	91.02
	R	100.00	98.79	90.30	81.21	95.73	93.33	64.24	98.79	75.15	97.58	64.02	98.12	73.62	66.07	98.54	99.34	98.68	96.45	88.67	88.35
	F1	97.06	96.45	91.98	86.73	94.86	93.62	75.44	96.45	82.94	95.83	75.27	96.02	81.91	76.29	96.09	96.46	96.15	94.77	90.78	90.27

we apply chain-of-thought prompts (Figure 5) that guide step-by-step inspection for AI-generated artifacts. For BusterX++, we follow its original prompt [73] to align with its evaluation setups. We report accuracy, recall, and F1-score on both our benchmark and GenVideo [5].

5.2. Main Results

Results on Our Benchmark. We compare with three baseline groups: (1) Binary detectors including AIGVDet [1], DeMamba [5], and the recent NSG-VD [84]. (2) Off-the-shelf MLLMs including VideoLLaMa-3 [82], Qwen2.5-VL series [2], InternVL-3 [69], GPT-4.1-mini [48], and Gemini-2.5-flash [11]. (3) MLM-based detector, i.e., BusterX++ [73] which is the only open-sourced implementation available. Table 1 shows our model consistently outperforms all baselines, achieving **+26.73%** absolute accuracy and **+17.27%** F1 over the second-best DeMamba. Compared to MLLM baselines, we notably achieve **+34.12%** accuracy, **+24.57%**

recall, and **+32%** F1. Our RL training further improves over SFT, especially on hard I2V samples, with **+3.74%** on recall.

Results on GenVideo Benchmark. GenVideo serves as our out-of-domain test, containing low-quality samples from outdated generators with near-static content [7]. Our model achieves **+11.07%** accuracy over the best binary detector and **+7.8%** accuracy, **+16.9%** recall over Skyra-SFT, as shown in Table 2. To demonstrate the ability to quickly adapt to OOD scenarios, we initialize our framework with Skyra-SFT and perform RL training on only 2.2K data randomly selected from the GenVideo-100K training set, following the “many-to-many” settings in GenVideo [5]. The RL training process, without any additional human-annotation, and is trained for only 1 epoch, quickly adapting Shyra to such a new domain, with the resulting model Skyra-RL-GenVideo achieving a **+19.22%** accuracy, **+42.06%** recall, and **+31%** F1-score gain than Skyra-RL.

Robustness Study. Real-world videos are usually repre-

Table 2. Detection performances on GenVideo.

Method	Metric	Model Scope	Morph Studio	Moon Valley	Hot Shot	Show1	Gen2	Crafter	Lavie	Sora	Wild Scrape	Avg.
AIGVDet	ACC	50.36	50.21	50.00	50.07	50.00	50.00	50.18	50.04	50.00	50.00	50.09
	R	0.71	0.43	0.00	0.14	0.00	0.00	0.36	0.07	0.00	0.00	0.17
	F1	1.42	0.28	0.00	0.29	0.00	0.00	0.71	0.14	0.00	0.00	0.34
DeMamba	ACC	<u>62.00</u>	61.36	62.06	56.36	<u>61.50</u>	62.75	61.80	61.29	62.50	55.51	60.71
	R	<u>96.43</u>	<u>98.43</u>	99.84	99.84	<u>85.57</u>	<u>97.14</u>	<u>98.91</u>	<u>98.86</u>	<u>97.93</u>	<u>88.11</u>	<u>95.94</u>
	F1	<u>71.32</u>	<u>71.81</u>	72.46	66.22	<u>71.61</u>	<u>72.65</u>	72.13	71.67	72.37	<u>66.45</u>	<u>70.91</u>
NSG-VD	ACC	49.79	50.14	49.60	50.29	50.07	50.22	49.86	50.29	50.00	40.94	49.12
	R	99.14	99.29	<u>98.88</u>	<u>99.14</u>	99.43	99.28	99.00	99.21	100.00	99.36	99.27
	F1	66.38	66.57	66.24	<u>66.60</u>	66.57	66.60	66.38	66.62	66.67	57.86	65.65
Ours-SFT(7B)	ACC	52.71	62.07	69.01	53.21	51.64	66.99	77.04	67.86	77.86	61.62	63.98
	R	6.14	24.43	38.98	7.00	4.86	34.64	54.72	36.29	55.36	24.56	28.70
	F1	11.50	39.18	55.17	13.01	9.13	51.21	70.44	53.03	71.26	39.02	41.00
Ours-RL(7B)	ACC	57.21	<u>69.14</u>	<u>81.71</u>	<u>57.50</u>	56.71	<u>75.94</u>	<u>86.16</u>	<u>78.50</u>	<u>86.61</u>	<u>68.34</u>	<u>71.78</u>
	R	16.71	40.29	65.34	17.57	16.57	54.49	73.75	59.14	73.21	38.88	45.60
	F1	28.09	56.63	<u>78.13</u>	29.25	27.68	69.37	<u>84.20</u>	<u>73.34</u>	<u>84.54</u>	55.11	59.00
Ours-RL-GenVideo(7B)	ACC	79.93	94.43	96.09	88.50	83.50	95.25	95.92	94.32	95.54	86.56	91.00
	R	66.29	95.86	97.92	82.71	72.00	96.23	98.07	94.29	95.64	78.63	87.66
	F1	76.76	94.51	96.16	87.79	81.36	95.30	96.01	94.32	95.50	85.41	90.00

Table 3. Robustness evaluation of different detectors on ViF-Bench.

Method	Metric	Origin	Compression	Transformation	Gaussian Noise	Light-transform		Color-transform	
						(-)	(+)	(-)	(+)
AIGVDet	ACC	69.08	70.33	54.91	56.30	62.33	64.01	72.93	77.52
	R	44.88	50.42	0.57	5.57	20.84	22.87	54.83	64.88
	F1	56.76	58.43	1.03	8.57	30.21	33.13	62.18	69.25
DeMamba	ACC	64.29	63.94	64.62	63.18	64.06	62.81	63.25	63.69
	R	96.66	96.68	<u>96.79</u>	<u>96.41</u>	<u>96.92</u>	<u>96.90</u>	96.55	96.81
	F1	73.00	72.28	72.69	71.80	72.40	71.71	71.88	72.18
NSG-VD	ACC	49.65	48.71	48.60	48.97	48.71	49.14	48.73	49.21
	R	98.66	99.20	98.97	99.72	99.19	98.80	99.22	98.94
	F1	66.21	65.34	65.24	65.58	65.34	65.44	65.35	65.50
Qwen-2.5-VL(7B)	ACC	51.26	49.95	48.93	50.68	48.93	54.90	48.93	54.94
	R	6.99	4.16	5.12	5.15	5.13	10.41	5.13	10.48
	F1	12.44	7.60	9.04	9.41	9.04	17.20	9.04	17.31
Buster-X++(7B)	ACC	56.90	55.02	59.10	59.54	59.12	54.90	59.12	54.94
	R	14.40	10.64	23.04	23.27	23.04	10.41	23.04	10.48
	F1	21.94	17.43	33.09	33.04	33.09	17.20	33.09	17.31
Ours-SFT(7B)	ACC	<u>90.11</u>	<u>80.52</u>	86.21	83.70	88.67	<u>88.12</u>	88.50	<u>88.51</u>
	R	84.65	85.54	91.31	94.77	89.93	80.68	85.21	80.85
	F1	88.76	<u>81.06</u>	86.64	<u>85.28</u>	88.51	<u>86.18</u>	87.43	<u>86.58</u>
Ours-RL(7B)	ACC	91.02	80.80	<u>83.26</u>	<u>83.48</u>	<u>83.26</u>	90.66	<u>83.26</u>	90.67
	R	88.35	88.64	96.37	96.34	96.37	85.78	96.37	85.81
	F1	90.27	81.93	<u>85.17</u>	85.33	<u>85.17</u>	89.62	<u>85.17</u>	89.64

sented in degraded formats, causing potential perturbations on the detecting performance. We evaluate robustness under five degradation types: Compression (JPEG), Transformation (Zoom), Gaussian Noise, Light Transform (-/+), and color-transform (-/+). Table 3 shows our model maintains state-of-the-art performance under all degradations.

5.3. Ablation Study

We conduct ablation studies to validate the effectiveness of our design, as shown in Table. 4

Effects of Training Strategies: Both the CoT reasoning process and the RL boost model’s detection performance.

In this part, we comprehensively evaluate the effectiveness of our method design by conducting the following ablation

Table 4. Results of ablation studies.

No.	Type	Ours-SFT			Ours-RL		
		Acc	R	F1	Acc	R	F1
		90.11	84.65	88.76	91.02	88.35	90.27
Ablation-I	wo CoT	54.04 (-36.07)	9.36 (-75.29)	16.72 (-72.04)	\	\	\
	w/o Cold-Start	\	\	\	50.09 (-40.93)	0.18 (-88.17)	0.37 (-89.90)
	w/o RL	\	\	\	90.11 (-0.91)	84.65 (-3.70)	88.76 (-1.51)
Ablation-II	wo Asymmetric Reward	\	\	\	76.24 (-14.78)	99.07 (+10.72)	80.65 (-9.62)
	wo Inspection Reward	\	\	\	90.05 (-0.97)	87.55 (-0.80)	89.30 (-0.97)

studies: (1) Without CoT in answer: we trained our model to answer with “Real/Fake” when inquired “Is the video a real or fake video?”. This naive implementation yields near-random performance. Without careful reasoning, the model cannot learn detection signals. (2) Without cold-start: we train the base model to perform AIGC video detection and explanation by CoT prompting and GRPO-based reinforcement learning using the design in Section. 4.3. While similar approaches, as introduced by DeepSeek-R1-Zero [18], have proven to be effective in various visual tasks [61, 64], duplicating its success to our tasks is not naive. The resulting model achieves even worse performance than (1). Considering the base model’s inability in AI-generated video detection tasks, purely RL can hardly equip the model with sufficient artifacts identifying capability without our cold-start initialization process [81]. (3) Without the RL stage: our reinforcement training stage further boosts the detection performance of the supervised finetuned model.

Effect of Reward Design: Direct real-fake binary reward yields suboptimal performance. In our reward score, we introduce two special designs: asymmetric accuracy reward and inspection reward. When setting the accuracy reward to 0.0 for both false positive and negative, the model quickly overfitted to “fake”, with a sharp decline in both accuracy (-14.78%) and F1-score (-9.62%). We also observe a performance drop when we replace the inspection reward with the normal format reward that only inspects whether the model’s response follows F_{outer} .

5.4. Case Study of the Explanation Ability

We provide two response cases of Skyra to demonstrate the explanation ability in Figure 6. Our analysis is as follows: (a) Through our cold-start initialization stage with our high-quality human-annotated dataset, and the RL stage training, which further enhances our model’s artifacts perception capability, we are delighted to find that Skyra can perceive tiny-grained AIGC evidence that are even hard for humans to identify. (b) For real videos, Skyra follows a “description-inspection-review-conclusion” process, which guides the model’s attention to those areas that are likely to contain artifact evidence, avoiding missing any possible forgery evidence, balancing the training process gap between real and AIGC videos, and also making the model’s explanation more



Figure 6. Case Study. More examples are provided in the appendix. persuasive. We provide more cases in the Appendix.

6. Conclusion and Discussions

In this paper, we introduce Skyra, a specialized multimodal large language model designed for interpretable, artifact-centric AI-generated video detection. Built upon the fine-grained, human-annotated ViF-CoT-4K dataset and a two-stage training pipeline that integrates supervised initialization with reinforcement learning, Skyra exhibits strong spatio-temporal artifact perception and produces coherent, grounded explanations. Extensive experiments on ViF-Bench and GenVideo demonstrate substantial improvements over existing binary and MLLM-based detectors, while also uncovering systematic patterns in generative artifacts and model reasoning behavior. We hope that Skyra, together with our dataset and benchmark, can support future research toward more transparent, robust, and trustworthy AIGC video detection systems, contributing to the broader effort of mitigating societal risks associated with synthetic media.

Limitations. Our training data are still bound by the specific generators and collection pipeline used in ViF-CoT-4K and ViF-Bench. Although we cover a diverse set of recent text-to-video and image-to-video models, the benchmark does not yet encompass all emerging media distributions (e.g., ultra-

long videos or non-photorealistic, stylized content). Also, Skyra does not assess the intent, context, or potential societal harm of a video. Its natural-language rationales are designed to be persuasive and human-readable, but they may still be overconfident or partially hallucinated. This highlights the importance of calibrated uncertainty estimation, human-in-the-loop use, and complementary safeguards when deploying such models in safety-critical scenarios.

Acknowledgement

This work was supported in part by the National Natural Science Foundation of China under Grant 62441616, Grant 62336004, Grant 62125603, Grant 62306031, Grant 62506198, in part by the China Postdoctoral Science Foundation under Grant 2024M761674.

References

- [1] Jianfa Bai, Man Lin, Gang Cao, and Zijie Lou. Ai-generated video detection via spatial-temporal anomaly learning. In *Chinese Conference on Pattern Recognition and Computer Vision (PRCV)*, pages 460–470. Springer, 2024. 1, 2, 5, 7
- [2] Shuai Bai, Keqin Chen, Xuejing Liu, Jialin Wang, Wenbin Ge, Sibao Song, Kai Dang, Peng Wang, Shijie Wang, Jun Tang, et al. Qwen2. 5-vl technical report. *arXiv preprint arXiv:2502.13923*, 2025. 1, 2, 4, 6, 7
- [3] Andreas Blattmann, Tim Dockhorn, Sumith Kulal, Daniel Mendelevitch, Maciej Kilian, Dominik Lorenz, Yam Levi, Zion English, Vikram Voleti, Adam Letts, et al. Stable video diffusion: Scaling latent video diffusion models to large datasets. *arXiv preprint arXiv:2311.15127*, 2023. 1, 4
- [4] Guibin Chen, Dixuan Lin, Jiangping Yang, Chunze Lin, Junchen Zhu, Mingyuan Fan, Hao Zhang, Sheng Chen, Zheng Chen, Chengcheng Ma, et al. Skyreels-v2: Infinite-length film generative model. *arXiv preprint arXiv:2504.13074*, 2025. 4
- [5] Haoxing Chen, Yan Hong, Zizheng Huang, Zhuoer Xu, Zhangxuan Gu, Yaohui Li, Jun Lan, Huijia Zhu, Jianfu Zhang, Weiqiang Wang, et al. Demamba: Ai-generated video detection on million-scale genvideo benchmark. *arXiv preprint arXiv:2405.19707*, 2024. 1, 2, 3, 4, 5, 7, 18
- [6] Tsai-Shien Chen, Aliaksandr Siarohin, Willi Menapace, Ekaterina Deyneka, Hsiang-wei Chao, Byung Eun Jeon, Yuwei Fang, Hsin-Ying Lee, Jian Ren, Ming-Hsuan Yang, et al. Panda-70m: Captioning 70m videos with multiple cross-modality teachers. In *Proceedings of the IEEE/CVF Conference on Computer Vision and Pattern Recognition*, pages 13320–13331, 2024. 4, 21
- [7] Weiliang Chen, Wenzhao Zheng, Yu Zheng, Lei Chen, Jie Zhou, Jiwen Lu, and Yueqi Duan. Genworld: Towards detecting ai-generated real-world simulation videos. *arXiv preprint arXiv:2506.10975*, 2025. 1, 2, 3, 4, 5, 7
- [8] Yize Chen, Zhiyuan Yan, Guangliang Cheng, Kangran Zhao, Siwei Lyu, and Baoyuan Wu. X2-dfd: A framework for explainable and extendable deepfake detection. *arXiv preprint arXiv:2410.06126*, 2024. 1, 2
- [9] Yukang Chen, Wei Huang, Baifeng Shi, Qinghao Hu, Hanrong Ye, Ligeng Zhu, Zhijian Liu, Pavlo Molchanov, Jan Kautz, Xiaojuan Qi, et al. Scaling rl to long videos. *arXiv preprint arXiv:2507.07966*, 2025. 3
- [10] Zhe Chen, Jiannan Wu, Wenhai Wang, Weijie Su, Guo Chen, Sen Xing, Muyan Zhong, Qinglong Zhang, Xizhou Zhu, Lewei Lu, et al. Internvl: Scaling up vision foundation models and aligning for generic visual-linguistic tasks. In *Proceedings of the IEEE/CVF conference on computer vision and pattern recognition*, pages 24185–24198, 2024. 2, 4
- [11] Google DeepMind. Gemini 2.5: Our most intelligent ai model. <https://blog.google/technology/google-deepmind/gemini-model-thinking-updates-march-2025/>, 2025. Accessed: 2025-11-14. 1, 4, 5, 6, 7, 19
- [12] Google DeepMind. Veo 3: Advanced generative video model. <https://aistudio.google.com/models/veo-3>, 2025. Accessed: 2025-11-14. 1, 3
- [13] Kaituo Feng, Kaixiong Gong, Bohao Li, Zonghao Guo, Yibing Wang, Tianshuo Peng, Junfei Wu, Xiaoying Zhang, Benyou Wang, and Xiangyu Yue. Video-r1: Reinforcing video reasoning in mllms. *arXiv preprint arXiv:2503.21776*, 2025. 3, 6
- [14] Shenghao Fu, Qize Yang, Yuan-Ming Li, Xihan Wei, Xiaohua Xie, and Wei-Shi Zheng. Love-r1: Advancing long video understanding with an adaptive zoom-in mechanism via multi-step reasoning. *arXiv preprint arXiv:2509.24786*, 2025. 3
- [15] Xingyu Fu, Siyi Liu, Yongkang Xu, et al. Learning human-perceived fakeness in ai-generated videos via multimodal llms. *arXiv preprint arXiv:2509.22646*, 2025. 2
- [16] Yifeng Gao, Yifan Ding, Hongyu Su, Juncheng Li, Yunhan Zhao, Lin Luo, Zixing Chen, Li Wang, Xin Wang, Yixu Wang, et al. David-xr1: Detecting ai-generated videos with explainable reasoning. *arXiv preprint arXiv:2506.14827*, 2025. 1, 2, 4
- [17] Dong Guo, Faming Wu, Feida Zhu, Fuxing Leng, Guang Shi, Haobin Chen, Haoqi Fan, Jian Wang, Jianyu Jiang, Jiawei Wang, et al. Seed1. 5-vl technical report. *arXiv preprint arXiv:2505.07062*, 2025. 3
- [18] Daya Guo, Dejian Yang, Haowei Zhang, Junxiao Song, Ruoyu Zhang, Runxin Xu, Qihao Zhu, Shirong Ma, Peiyi Wang, Xiao Bi, et al. Deepseek-r1: Incentivizing reasoning capability in llms via reinforcement learning. *arXiv preprint arXiv:2501.12948*, 2025. 6, 9
- [19] Shasha Guo, Liang Pang, Xi Wang, Yanling Wang, Huawei Shen, and Jing Zhang. Geovlmath: Enhancing geometry reasoning in vision-language models via cross-modal reward for auxiliary line creation. *arXiv preprint arXiv:2510.11020*, 2025. 3
- [20] Xiao Guo, Xiufeng Song, Yue Zhang, Xiaohong Liu, and Xiaoming Liu. Rethinking vision-language model in face forensics: Multi-modal interpretable forged face detector. In *Proceedings of the Computer Vision and Pattern Recognition Conference*, pages 105–116, 2025. 1, 2
- [21] Yoav HaCohen, Nisan Chiprut, Benny Brazowski, Daniel Shalem, Dudu Moshe, Eitan Richardson, Eran Levin, Guy Shiran, Nir Zabari, Ori Gordon, et al. Ltx-video: Realtime video latent diffusion. *arXiv preprint arXiv:2501.00103*, 2024. 4, 5
- [22] Zefeng He, Xiaoye Qu, Yafu Li, Siyuan Huang, Daizong Liu, and Yu Cheng. Framethinker: Learning to think with long videos via multi-turn frame spotlighting. *arXiv preprint arXiv:2509.24304*, 2025. 3
- [23] Wenyi Hong, Ming Ding, Wendi Zheng, Xinghan Liu, and Jie Tang. Cogvideo: Large-scale pretraining for text-to-video generation via transformers. *arXiv preprint arXiv:2205.15868*, 2022. 4
- [24] Yushi Hu, Weijia Shi, Xingyu Fu, Dan Roth, Mari Ostendorf, Luke Zettlemoyer, Noah A Smith, and Ranjay Krishna. Visual sketchpad: Sketching as a visual chain of thought for multimodal language models. *Advances in Neural Information Processing Systems*, 37:139348–139379, 2024. 3
- [25] Aaron Hurst, Adam Lerer, Adam P Goucher, Adam Perelman, Aditya Ramesh, Aidan Clark, AJ Ostrow, Akila Welihinda, Alan Hayes, Alec Radford, et al. Gpt-4o system card. *arXiv preprint arXiv:2410.21276*, 2024. 1, 2, 4

- [26] Christian Internò, Robert Geirhos, Markus Olhofer, Sunny Liu, Barbara Hammer, and David Klindt. Ai-generated video detection via perceptual straightening. *arXiv preprint arXiv:2507.00583*, 2025. 1, 2, 5
- [27] Zeyinzi Jiang, Zhen Han, Chaojie Mao, Jingfeng Zhang, Yulin Pan, and Yu Liu. Vace: All-in-one video creation and editing. *arXiv preprint arXiv:2503.07598*, 2025. 4
- [28] Hengrui Kang, Siwei Wen, Zichen Wen, Junyan Ye, Weijia Li, Peilin Feng, Baichuan Zhou, Bin Wang, Dahua Lin, Linfeng Zhang, et al. Legion: Learning to ground and explain for synthetic image detection. *arXiv preprint arXiv:2503.15264*, 2025. 2
- [29] Will Kay, Joao Carreira, Karen Simonyan, Brian Zhang, Chloe Hillier, Sudheendra Vijayanarasimhan, Fabio Viola, Tim Green, Trevor Back, Paul Natsev, et al. The kinetics human action video dataset. *arXiv preprint arXiv:1705.06950*, 2017. 4, 21
- [30] Levon Khachatryan, Andranik Movsisyan, Vahram Tadevosyan, Roberto Henschel, Zhangyang Wang, Shant Navasardyan, and Humphrey Shi. Text2video-zero: Text-to-image diffusion models are zero-shot video generators. In *Proceedings of the IEEE/CVF International Conference on Computer Vision*, pages 15954–15964, 2023. 4
- [31] KlingAI. Klingai: Creative video generation platform. <https://klingai.com/>, 2025. Accessed: 2025-11-14. 1, 4
- [32] Weijie Kong, Qi Tian, Zijian Zhang, Rox Min, Zuozhuo Dai, Jin Zhou, Jiangfeng Xiong, Xin Li, Bo Wu, Jianwei Zhang, et al. Hunyuanvideo: A systematic framework for large video generative models. *arXiv preprint arXiv:2412.03603*, 2024. 1, 4, 5
- [33] Xin Lai, Junyi Li, Wei Li, Tao Liu, Tianjian Li, and Hengshuang Zhao. Mini-o3: Scaling up reasoning patterns and interaction turns for visual search. *arXiv preprint arXiv:2509.07969*, 2025. 3
- [34] Junnan Li, Dongxu Li, Silvio Savarese, and Steven Hoi. Blip-2: Bootstrapping language-image pre-training with frozen image encoders and large language models. In *International conference on machine learning*, pages 19730–19742. PMLR, 2023. 1
- [35] Kunchang Li, Yali Wang, Yanan He, Yizhuo Li, Yi Wang, Yi Liu, Zun Wang, Jilan Xu, Guo Chen, Ping Luo, et al. Mvbench: A comprehensive multi-modal video understanding benchmark. In *Proceedings of the IEEE/CVF Conference on Computer Vision and Pattern Recognition*, pages 22195–22206, 2024. 3
- [36] Xinhao Li, Ziang Yan, Desen Meng, Lu Dong, Xiangyu Zeng, Yanan He, Yali Wang, Yu Qiao, Yi Wang, and Limin Wang. Videochat-r1: Enhancing spatio-temporal perception via reinforcement fine-tuning. *arXiv preprint arXiv:2504.06958*, 2025. 6
- [37] Yixuan Li, Xuelin Liu, Xiaoyang Wang, Bu Sung Lee, Shiqi Wang, Anderson Rocha, and Weisi Lin. Fakebench: Probing explainable fake image detection via large multimodal models. *IEEE Transactions on Information Forensics and Security*, 2025. 1
- [38] Haotian Liu, Chunyuan Li, Qingyang Wu, and Yong Jae Lee. Visual instruction tuning. *Advances in neural information processing systems*, 36:34892–34916, 2023. 1, 2
- [39] Yuqi Liu, Bohao Peng, Zhisheng Zhong, Zihao Yue, Fanbin Lu, Bei Yu, and Jiaya Jia. Seg-zero: Reasoning-chain guided segmentation via cognitive reinforcement. *arXiv preprint arXiv:2503.06520*, 2025. 3
- [40] Long Ma, Jiajia Zhang, Hongping Deng, Ningyu Zhang, Qinglang Guo, Haiyang Yu, Yong Liao, and Pengyuan Zhou. Decof: Generated video detection via frame consistency: The first benchmark dataset. *arXiv e-prints*, pages arXiv–2402, 2024. 2
- [41] Muhammad Maaz, Hanoona Rasheed, Salman Khan, and Fahad Shahbaz Khan. Video-chatgpt: Towards detailed video understanding via large vision and language models. *arXiv preprint arXiv:2306.05424*, 2023. 3
- [42] Jiahao Meng, Xiangtai Li, Haochen Wang, Yue Tan, Tao Zhang, Lingdong Kong, Yunhai Tong, Anran Wang, Zhiyang Teng, Yujing Wang, et al. Open-o3 video: Grounded video reasoning with explicit spatio-temporal evidence. *arXiv preprint arXiv:2510.20579*, 2025. 6
- [43] MiniMax. Hailuo 02: Global ai video generation model by minimax. <https://hailuo-02.com/>, 2025. Accessed: 2025-11-14. 4, 5
- [44] Zhenliang Ni, Qiangyu Yan, Mouxiao Huang, Tianning Yuan, Yehui Tang, Hailin Hu, Xinghao Chen, and Yunhe Wang. Genvidbench: A challenging benchmark for detecting ai-generated video. *arXiv preprint arXiv:2501.11340*, 2025. 1, 2, 3, 4
- [45] Junbo Niu, Yifei Li, Ziyang Miao, Chunjiang Ge, Yuanhang Zhou, Qihao He, Xiaoyi Dong, Haodong Duan, Shuangrui Ding, Rui Qian, et al. Ovo-bench: How far is your video-llms from real-world online video understanding? In *Proceedings of the Computer Vision and Pattern Recognition Conference*, pages 18902–18913, 2025. 3
- [46] OpenAI. Gpt-4o mini: Advancing cost-efficient intelligence. <https://openai.com/index/gpt-4o-mini-advancing-cost-efficient-intelligence/>, 2024. Accessed: 2025-11-14. 4, 17
- [47] OpenAI. Sora 2 is here: Next-generation video-and-audio generation model. <https://openai.com/index/sora-2/>, 2025. Accessed: 2025-11-14. 1, 3, 4, 5
- [48] OpenAI. Introducing gpt-4.1 in the api. <https://openai.com/index/gpt-4-1/>, 2025. Accessed: 2025-11-14. 1, 4, 6, 7
- [49] Kyoungjun Park, Yifan Yang, Juheon Yi, Shicheng Zheng, Yifei Shen, Dongqi Han, Caihua Shan, Muhammad Muaz, and Lili Qiu. Vidguard-r1: Ai-generated video detection and explanation via reasoning mllms and rl. *arXiv preprint arXiv:2510.02282*, 2025. 1, 2, 4
- [50] William Peebles and Saining Xie. Scalable diffusion models with transformers. In *Proceedings of the IEEE/CVF international conference on computer vision*, pages 4195–4205, 2023. 1
- [51] Pika Art. Pika.art. <https://pika.art/>, 2025. Accessed: 2025-11-14. 4
- [52] PixVerse AI. Pixverse – ai video generator from text & photos. <https://app.pixverse.ai/>, 2025. Accessed: 2025-11-14. 4

- [53] Qwen Team. Qwen3-vl: Sharper vision, deeper thought, broader action. <https://qwen.ai/blog?id=99f0335c4ad9ff6153e517418d48535ab6d8afef&from=research.latest-advancements-list>, 2025. Accessed: 2025-10-23. 1, 3
- [54] Runway AI, Inc. Introducing runway gen-4. <https://runwayml.com/research/introducing-runway-gen-4>, 2025. Accessed: 2025-11-14. 4
- [55] Zhihong Shao, Peiyi Wang, Qihao Zhu, Runxin Xu, Junxiao Song, Xiao Bi, Haowei Zhang, Mingchuan Zhang, YK Li, Yang Wu, et al. Deepseekmath: Pushing the limits of mathematical reasoning in open language models. *arXiv preprint arXiv:2402.03300*, 2024. 6
- [56] Roger N Shepard. Perceptual-cognitive universals as reflections of the world. *Psychonomic Bulletin & Review*, 1(1): 2–28, 1994. 5
- [57] Mohamed R Shoaib, Zefan Wang, Milad Taleby Ahvanooe, and Jun Zhao. Deepfakes, misinformation, and disinformation in the era of frontier ai, generative ai, and large ai models. In *2023 international conference on computer and applications (ICCA)*, pages 1–7. IEEE, 2023. 1
- [58] Elizabeth Spelke. Initial knowledge: Six suggestions. *Cognition*, 50(1-3):431–445, 1994. 5
- [59] Elizabeth S Spelke and Katherine D Kinzler. Core knowledge. *Developmental science*, 10(1):89–96, 2007. 5
- [60] Zhaochen Su, Linjie Li, Mingyang Song, Yunzhuo Hao, Zhengyuan Yang, Jun Zhang, Guanjie Chen, Jiawei Gu, Juntao Li, Xiaoye Qu, et al. Openthinking: Learning to think with images via visual tool reinforcement learning. *arXiv preprint arXiv:2505.08617*, 2025. 3
- [61] Zhaochen Su, Peng Xia, Hangyu Guo, Zhenhua Liu, Yan Ma, Xiaoye Qu, Jiaqi Liu, Yanshu Li, Kaide Zeng, Zhengyuan Yang, et al. Thinking with images for multimodal reasoning: Foundations, methods, and future frontiers. *arXiv preprint arXiv:2506.23918*, 2025. 3, 9
- [62] Zhihao Sun, Haoran Jiang, Haoran Chen, Yixin Cao, Xipeng Qiu, Zuxuan Wu, and Yu-Gang Jiang. Forgerysluth: Empowering multimodal large language models for image manipulation detection. *arXiv preprint arXiv:2411.19466*, 2024. 2
- [63] Hao Tan, Jun Lan, Zichang Tan, Ajian Liu, Chuanbiao Song, Senyuan Shi, Huijia Zhu, Weiqiang Wang, Jun Wan, and Zhen Lei. Veritas: Generalizable deepfake detection via pattern-aware reasoning. *arXiv preprint arXiv:2508.21048*, 2025. 1, 2
- [64] Yunlong Tang, Jing Bi, Pinxin Liu, Zhenyu Pan, Zhangyuan Tan, Qianxiang Shen, Jiani Liu, Hang Hua, Junjia Guo, Yunzhong Xiao, et al. Video-llm post-training: A deep dive into video reasoning with large multimodal models. *arXiv preprint arXiv:2510.05034*, 2025. 3, 9
- [65] Gemini Team, Rohan Anil, Sebastian Borgeaud, Jean-Baptiste Alayrac, Jiahui Yu, Radu Soricut, Johan Schalkwyk, Andrew M Dai, Anja Hauth, Katie Millican, et al. Gemini: a family of highly capable multimodal models. *arXiv preprint arXiv:2312.11805*, 2023. 2
- [66] Team Wan, Ang Wang, Baole Ai, Bin Wen, Chaojie Mao, Chen-Wei Xie, Di Chen, Feiwei Yu, Haiming Zhao, Jianxiao Yang, et al. Wan: Open and advanced large-scale video generative models. *arXiv preprint arXiv:2503.20314*, 2025. 1, 3, 4, 5
- [67] Jiuniu Wang, Hangjie Yuan, Dayou Chen, Yingya Zhang, Xiang Wang, and Shiwei Zhang. Modelscope text-to-video technical report. *arXiv preprint arXiv:2308.06571*, 2023. 4
- [68] Peng Wang, Shuai Bai, Sinan Tan, Shijie Wang, Zhihao Fan, Jinze Bai, Keqin Chen, Xuejing Liu, Jialin Wang, Wenbin Ge, et al. Qwen2-vl: Enhancing vision-language model’s perception of the world at any resolution. *arXiv preprint arXiv:2409.12191*, 2024. 2, 3
- [69] Weiyun Wang, Zhangwei Gao, Lixin Gu, Hengjun Pu, Long Cui, Xingguang Wei, Zhaoyang Liu, Linglin Jing, Shenglong Ye, Jie Shao, et al. Internvl3. 5: Advancing open-source multimodal models in versatility, reasoning, and efficiency. *arXiv preprint arXiv:2508.18265*, 2025. 3, 6, 7
- [70] Weihang Wang, Zehai He, Wenyi Hong, Yean Cheng, Xiaohan Zhang, Ji Qi, Ming Ding, Xiaotao Gu, Shiyu Huang, Bin Xu, et al. Lvbench: An extreme long video understanding benchmark. In *Proceedings of the IEEE/CVF International Conference on Computer Vision*, pages 22958–22967, 2025. 3
- [71] Jason Wei, Xuezhi Wang, Dale Schuurmans, Maarten Bosma, Fei Xia, Ed Chi, Quoc V Le, Denny Zhou, et al. Chain-of-thought prompting elicits reasoning in large language models. *Advances in neural information processing systems*, 35:24824–24837, 2022. 1, 5
- [72] Haiquan Wen, Yiwei He, Zhenglin Huang, Tianxiao Li, Zihan Yu, Xingru Huang, Lu Qi, Baoyuan Wu, Xiangtai Li, and Guangliang Cheng. Busterx: Mllm-powered ai-generated video forgery detection and explanation. *arXiv preprint arXiv:2505.12620*, 2025. 1, 2, 3, 4, 19
- [73] Haiquan Wen, Tianxiao Li, Zhenglin Huang, Yiwei He, and Guangliang Cheng. Busterx++: Towards unified cross-modal ai-generated content detection and explanation with mllm. *arXiv preprint arXiv:2507.14632*, 2025. 1, 2, 4, 6, 7, 19, 20
- [74] Siwei Wen, Junyan Ye, Peilin Feng, Hengrui Kang, Zichen Wen, Yize Chen, Jiang Wu, Wenjun Wu, Conghui He, and Weijia Li. Spot the fake: Large multimodal model-based synthetic image detection with artifact explanation. *arXiv preprint arXiv:2503.14905*, 2025. 2
- [75] Haoning Wu, Dongxu Li, Bei Chen, and Junnan Li. Longvideobench: A benchmark for long-context interleaved video-language understanding. *Advances in Neural Information Processing Systems*, 37:28828–28857, 2024. 3
- [76] Danni Xu, Shaojing Fan, and Mohan Kankanhalli. Combating misinformation in the era of generative ai models. In *Proceedings of the 31st ACM International Conference on Multimedia*, pages 9291–9298, 2023. 1
- [77] Zhipei Xu, Xuanyu Zhang, Runyi Li, Zecheng Tang, Qing Huang, and Jian Zhang. Fakeshield: Explainable image forgery detection and localization via multi-modal large language models. *arXiv preprint arXiv:2410.02761*, 2024. 2
- [78] Hongwei Xue, Tiankai Hang, Yanhong Zeng, Yuchong Sun, Bei Liu, Huan Yang, Jianlong Fu, and Baining Guo. Advancing high-resolution video-language representation with large-scale video transcriptions. In *Proceedings of the IEEE/CVF*

- Conference on Computer Vision and Pattern Recognition*, pages 5036–5045, 2022. 4, 21
- [79] Ziang Yan, Xinhao Li, Yinan He, Zhengrong Yue, Xiangyu Zeng, Yali Wang, Yu Qiao, Limin Wang, and Yi Wang. Videochat-r1. 5: Visual test-time scaling to reinforce multimodal reasoning by iterative perception. *arXiv preprint arXiv:2509.21100*, 2025. 3
- [80] Zhuoyi Yang, Jiayan Teng, Wendi Zheng, Ming Ding, Shiyu Huang, Jiazheng Xu, Yuanming Yang, Wenyi Hong, Xiaohan Zhang, Guanyu Feng, et al. Cogvideox: Text-to-video diffusion models with an expert transformer. *arXiv preprint arXiv:2408.06072*, 2024. 1, 3, 4, 5
- [81] Yang Yue, Zhiqi Chen, Rui Lu, Andrew Zhao, Zhaokai Wang, Shiji Song, and Gao Huang. Does reinforcement learning really incentivize reasoning capacity in llms beyond the base model? *arXiv preprint arXiv:2504.13837*, 2025. 9
- [82] Hang Zhang, Xin Li, and Lidong Bing. Video-llama: An instruction-tuned audio-visual language model for video understanding. *arXiv preprint arXiv:2306.02858*, 2023. 2, 3, 6, 7
- [83] Pan Zhang, Xiaoyi Dong, Yuhang Cao, Yuhang Zang, Rui Qian, Xilin Wei, Lin Chen, Yifei Li, Junbo Niu, Shuangrui Ding, et al. Internlm-xcomposer2. 5-omnilive: A comprehensive multimodal system for long-term streaming video and audio interactions. *arXiv preprint arXiv:2412.09596*, 2024. 2
- [84] Shuhai Zhang, Zihao Lian, Jiahao Yang, Daiyuan Li, Guoxuan Pang, Feng Liu, Bo Han, Shutao Li, and Mingkui Tan. Physics-driven spatiotemporal modeling for ai-generated video detection. *arXiv preprint arXiv:2510.08073*, 2025. 1, 2, 4, 5, 7, 18
- [85] Wayne Zhang, Changjiang Jiang, Zhonghao Zhang, Chenyang Si, Fengchang Yu, and Wei Peng. Ivy-fake: A unified explainable framework and benchmark for image and video aigc detection. *arXiv preprint arXiv:2506.00979*, 2025. 2, 4
- [86] Xintong Zhang, Zhi Gao, Bofei Zhang, Pengxiang Li, Xiaowen Zhang, Yang Liu, Tao Yuan, Yuwei Wu, Yunde Jia, Song-Chun Zhu, et al. Chain-of-focus: Adaptive visual search and zooming for multimodal reasoning via rl. *arXiv preprint arXiv:2505.15436*, 2025. 3
- [87] Yue Zhang, Ben Colman, Xiao Guo, Ali Shahriyari, and Gaurav Bharaj. Common sense reasoning for deepfake detection. In *European conference on computer vision*, pages 399–415. Springer, 2024. 1, 2, 5
- [88] Yanran Zhang, Wenzhao Zheng, Yifei Li, Bingyao Yu, Yu Zheng, Lei Chen, Jiwen Lu, and Jie Zhou. Unigendet: A unified generative-discriminative framework for co-evolutionary image generation and generated image detection. *arXiv preprint arXiv:2604.21904*, 2026. 2
- [89] Yi-Fan Zhang, Xingyu Lu, Shukang Yin, Chaoyou Fu, Wei Chen, Xiao Hu, Bin Wen, Kaiyu Jiang, Changyi Liu, Tianke Zhang, et al. Thyme: Think beyond images. *arXiv preprint arXiv:2508.11630*, 2025. 3
- [90] Chende Zheng, Ruiqi Suo, Chenhao Lin, Zhengyu Zhao, Le Yang, Shuai Liu, Minghui Yang, Cong Wang, and Chao Shen. D3: Training-free ai-generated video detection using second-order features. In *Proceedings of the IEEE/CVF International Conference on Computer Vision*, pages 12852–12862, 2025. 1, 2, 5
- [91] Ziwei Zheng, Michael Yang, Jack Hong, Chenxiao Zhao, Guohai Xu, Le Yang, Chao Shen, and Xing Yu. Deepeyes: Incentivizing "thinking with images" via reinforcement learning. *arXiv preprint arXiv:2505.14362*, 2025. 3
- [92] Yueying Zou, Peipei Li, Zekun Li, Huaibo Huang, Xing Cui, Xuannan Liu, Chenghanyu Zhang, and Ran He. Survey on ai-generated media detection: From non-mlm to mlm. *arXiv preprint arXiv:2502.05240*, 2025. 5

Appendix

Content of Appendices

Section A. The ViF Dataset.

- § A.1. Definition of Each Artifact Category.
- § A.2. Annotation Platform.
- § A.3. Chain-of-Thought Annotation Prompt Design.
- § A.4. Annotation Details, Dataset Statistics, and

Training Settings.

- § A.5. Detailed Statistics of ViF-CoT-4K.
- § A.6. Generated Video Examples.

Section B. Analysis of Generalization Ablations.

Section C. Analysis of Artifact Cues.

Section D. Analysis of Baselines' Detection Capabilities.

- § D.1. Binary Detectors.
- § D.2. Off-the-Shelf MLLMs.
- § D.3. Existing MLLM-based Detectors.

Section E. Additional Examples.

- § E.1. Design of Prompts.
- § E.2. Examples of Skyra's Responses.

Section F. Broader Impacts.

Section G. License.

A. The ViF Dataset

A.1. Definition of Each Artifact Category

We provide detailed definitions of each category in our artifact taxonomy (Section 3.2) as follows.

Low-Level Forgery. This group summarizes characteristic visual cues that frequently make current AI-generated videos appear “unnatural”. These cues typically do not explicitly violate physical laws, but reflect systematic limitations of mainstream video generation models.

- **Texture Anomaly.** This category focuses on abnormal patterns in local textures.
 - *Structure Anomaly.* Regions with rich structures (e.g., fences, grids, lattices) exhibit unnatural distortion, twisting, or interlacing, leading to inconsistent or implausible geometric patterns.
 - *Texture Jittering.* Surface textures show high-frequency flickering or drifting over time, manifesting as crawling patterns, grid-like noise, or temporally unstable blur, instead of stable, physically plausible textures.
 - *Unnatural Blur.* Blur and degradation patterns differ from typical natural degradations, such as Gaussian blur or compression artifacts. The blur may be spatially inconsistent, texture-selective, or temporally unstable in a way rarely observed in real videos.
- **Color and Lighting Anomaly.** This category captures implausible color or illumination patterns that deviate from natural imaging conditions.
 - *Color Over-saturation.* Certain regions exhibit excessively saturated or overly vivid colors (often in blue, red,

or green), with insufficient tonal variation or shading, making the area visually stand out unnaturally.

- *Lighting Inconsistency.* Global or local illumination changes abruptly or violently over time, or shows strong intensity fluctuations that cannot be explained by realistic changes of light sources, exposure, or scene configuration.
- **Motion Forgery.** This category describes unnatural camera-related motion patterns.
 - *Camera Motion Inconsistency.* The apparent camera motion is abnormal, such as erratic zooming in/out, unnatural high-frequency panning, or irregular shaking. These artifacts are often accompanied by inconsistent changes in object positions, scales, or spatial relations that do not match a physically plausible camera trajectory.

Violation of Laws. This group contains artifacts that clearly violate real-world constraints, including object permanence, physical laws, causality, and basic common sense. Detecting these cues generally requires spatio-temporal reasoning and background knowledge about how objects and scenes behave in reality.

- **Object Inconsistency.** This category focuses on violations of object permanence and identity over time.
 - *Abnormal Object Disappearance.* An object disappears suddenly during its motion without any plausible interaction or occlusion. For example, a runner on a track vanishes abruptly while continuing to move forward.
 - *Abnormal Object Appearance.* An object suddenly appears and starts to move without any reasonable cause or prior indication. For example, a new runner appears out of nowhere on the track in the middle of the video.
 - *Person Identity Inconsistency.* The identity of a person changes over time, especially in facial features or other stable identity cues. For example, a person's face disappears and reappears with clearly different facial characteristics, leading to a mismatch in perceived identity.
 - *General Object Identity Inconsistency.* The identity of a generic object changes significantly over time without any obvious external cause. For example, a chair being rotated by a person ends up with a drastically different color or structure compared to its initial state.
 - *Shape Distortion.* Rigid objects exhibit non-rigid deformations during motion. For instance, a human body suddenly scales up and down or undergoes frequent surface distortions and twisting that are incompatible with rigid-body motion.
- **Interaction Inconsistency.** This category captures physically implausible interactions between multiple objects.
 - *Abnormal Rigid-Body Crossing.* Rigid objects that should remain non-interpenetrating instead of intersecting or passing through each other. For example, a bar-

bell that should move in front of a person’s body passes unrealistically through the person’s head.

- *Abnormal Multi-Object Merging*. Two or more distinct objects gradually or abruptly merge into a single object during motion, without any plausible explanation (e.g., three people in motion merge into two).
- *Abnormal Object Splitting*. A single object splits into multiple distinct objects during motion, again without any reasonable cause (e.g., one person splits into two separate people).
- *General Interaction Anomaly*. Other abnormal or implausible phenomena occurring during interactions between two or more objects, such as missing collisions, inconsistent contact, or contradictory occlusion relations.
- **Unnatural Movement**. This category denotes motion patterns that contradict the typical kinematics of humans, animals, or objects.
 - *Unnatural Human Movement*. Human body motion deviates from normal biomechanics or everyday experience. For example, a person walks without leg crossing, exhibiting pure lateral sliding of the legs instead of realistic gait cycles.
 - *Unnatural Animal Movement*. Animal motion is incompatible with known locomotion patterns. For example, a running horse moves its hind legs in parallel translation without proper alternating strides.
 - *Unnatural General Object Movement*. Objects other than humans and animals follow trajectories or undergo transformations that are inconsistent with real-world dynamics, such as erratic acceleration, unnatural smoothness, or implausible temporal discontinuities.
- **Violation of Causality Law**. This category collects artifacts that violate physical laws or general causal relationships.
 - *Violation of Physical Laws*. The motion of objects contradicts basic physical principles, such as force–acceleration relationships or conservation laws. For example, a ball moves or changes velocity in the absence of any visible force, or instantaneously teleports at unrealistic speeds.
 - *Violation of General Causality Violation*. Events occur without observable causes, or actions fail to produce their expected effects. For example, a boy spills milk onto a table, but no milk traces appear on the table surface.
- **Violation of Common Sense**. This category covers structural or semantic inconsistencies that conflict with basic commonsense knowledge.
 - *Abnormal Human Body Structure*. The generated human body deviates from normal anatomical structure. Examples include extra or missing body parts (e.g., two heads, three or six fingers), or impossible body bending

that is incompatible with human physiology.

- *Abnormal General Object Structure*. Non-human objects exhibit structures that are inconsistent with their typical shapes or assembly, such as missing essential components or impossible connections.
- *Text Distortion*. Text appearing in the scene is severely distorted, malformed, or rendered as illegible gibberish without coherent semantic content, beyond mild degradation commonly observed in real footage.

A.2. Annotation Platform

Our annotation platform presents each AI-generated video alongside its corresponding real counterpart in a synchronized comparison view (Figure 7). This side-by-side layout allows annotators to directly contrast suspicious regions in the fake video with how the same scene should plausibly appear in real footage, making it easier to distinguish genuine physical phenomena from artifacts that only occur in AIGC videos. For every identified clue, annotators are required to select a fine-grained artifact category, provide detailed textual explanations for both the fake and real videos, and supply precise spatio-temporal annotations by marking time spans and bounding boxes in both streams. By enforcing mirrored annotations on fake–real pairs, the platform encourages annotators to explicitly encode both “what is wrong” in the generated video and “what is normal” in the real video, guiding the model toward learning an unbiased perceptual representation that treats real and synthetic content in a symmetric manner.

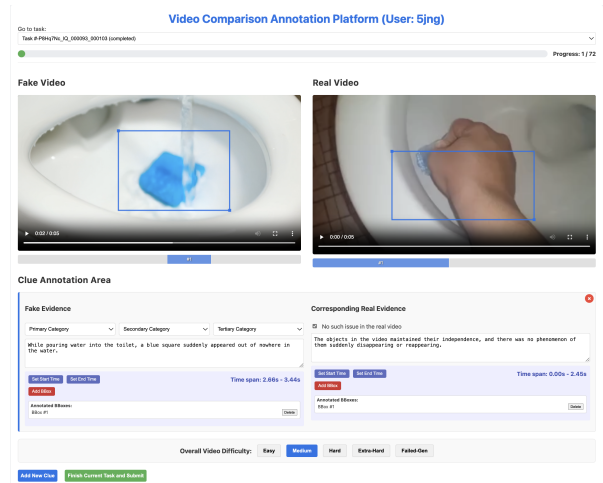


Figure 7. Annotation platform UI.

A.3. Chain-of-Thought Annotation Prompt Design

To transform concise human annotations into training-ready step-by-step supervision, we design a structured prompt for Gemini-2.5-Pro that operates on each fake–real video pair. For every annotated instance, the model receives sampled frames from the fake and real videos to

gether with the curated artifact **Type**, **Textual Explanation**, **Timestamps**, and **Bounding Boxes**, and is instructed to produce two independent CoT strings: one that carefully discovers all artifacts in the fake video and one that systematically clears the corresponding regions in the real video. The prompt enforces a standardized JSON output format (with separate `fake_cot_annotation` and `real_cot_annotation` fields), requires explicit tagging of temporal spans and spatial regions, and guides the reasoning process through an *observe-understand-draft-review-conclude* workflow with in-context examples. This design allows us to automatically expand precise but terse human labels into rich, consistent CoT supervision suitable for SFT. The complete prompt is provided in Figure 13

A.4. Annotation Details, Dataset Statistics, and Training Settings

We provide a comprehensive summary of dataset and training specifications in Table 5.

Annotation Protocol. A total of 25 trained professional annotators participated in the annotation process. Each annotator followed detailed guidelines covering artifact definitions (Section A.1), annotation platform usage (Section A.2), and quality standards. The annotation workflow proceeded as follows: (1) annotators watched each AI-generated video alongside its real counterpart in the synchronized comparison view (Figure 7); (2) for each identified artifact, they selected a fine-grained category from our taxonomy, provided textual explanations, and marked precise temporal spans and bounding boxes; (3) annotations underwent multiple review cycles to ensure quality and inter-annotator consistency.

Video Filtering. To ensure the quality and relevance of the collected videos, we apply a two-stage filtering pipeline: (i) *automatic semantic consistency checking* via GPT-4o-mini [46] between the AI-generated and real videos, which removes pairs with significant semantic drift; and (ii) *manual filtering* during annotation, where annotators remove static, ambiguous, or severely distorted samples that are unsuitable for meaningful artifact analysis.

A.5. Detailed Statistics of ViF-CoT-4K

We further reveal the statistic details of ViF-CoT-4K and ViF-Bench, including a detailed report of the proportion of different types of artifacts annotated in ViF-CoT-4K (Table. 9), and technical details of the video generation model in ViF-CoT-4K and ViF-Bench (Table. 10).

A.6. Generated Video Examples

We demonstrate the quality of our dataset and benchmark by showing several examples randomly selected from the ViF-Bench (Figures 14& 15). As shown in the image, fake samples in our dataset are generated by latest video generation

Table 5. Dataset and training specifications.

Dataset Statistics	
Video duration	5 seconds (real & fake, train & test)
Total frames per video	81 frames
Resolution	256p (short side)
Training Settings	
Sampled frames	16 frames per video (uniformly sampled)
Input resolution	256p (short side)
SFT learning rate	1e-5
SFT epochs	5
RL actor learning rate	5e-7
RL KL coefficient	0.02
Batch size per device	1
Hardware	8× NVIDIA H200 GPUs

Table 6. Generalization ablation study across in-generator, cross-generator, and cross-dataset settings on ViF-Bench and GenVideo.

Setting	In-Generators			Cross-Generators			Cross-Dataset		
	Acc	R	F1	Acc	R	F1	Acc	R	F1
w/o CoT	57.27	15.67	26.94	53.99	9.29	16.55	51.89	6.78	14.66
w/o SFT	70.91	87.27	75.00	75.87	98.82	80.36	<u>68.34</u>	<u>34.50</u>	<u>46.00</u>
Skyra-SFT	<u>92.62</u>	<u>89.49</u>	<u>92.13</u>	<u>88.95</u>	82.42	<u>87.20</u>	63.98	28.70	41.00
Skyra-RL	93.58	93.22	93.45	89.84	<u>86.10</u>	88.80	71.78	45.60	59.00

models, and are closely aligned with their real counterparts to mitigate their gap in semantics and format.

B. Analysis of Generalization Ablations.

Generalization Analysis: RL is the primary driver of cross-domain generalization. We further isolate each component’s contribution to generalization by evaluating under in-generator, cross-generator, and cross-dataset settings (Table 6). While SFT significantly improves in-domain accuracy, it also introduces mild overfitting, as cross-dataset accuracy drops from 68.34% to 63.98%. The subsequent RL stage recovers and extends generalization, yielding a +7.8% cross-dataset accuracy gain over SFT while preserving in-domain performance. This suggests that RL encourages the model to discover intrinsic artifact cues rather than generator-specific patterns.

C. Analysis of Artifact Cues

To provide insight into what visual and temporal cues Skyra relies on for detection, we analyze the distribution of artifacts detected by Skyra on ViF-Bench, as shown in Table 7.

Among all detected artifacts, 82.8% belong to *Violation of Laws* while only 17.2% are *Low-Level Forgery*, indicating that Skyra primarily performs semantic reasoning about physical and logical inconsistencies rather than relying on low-level generator fingerprints. Within the *Violation of Laws* category, *Object Inconsistency* accounts for 28.1%, with *Shape Distortion* (15.2%) being the single most dominant artifact type. This reflects a shared difficulty across cur-

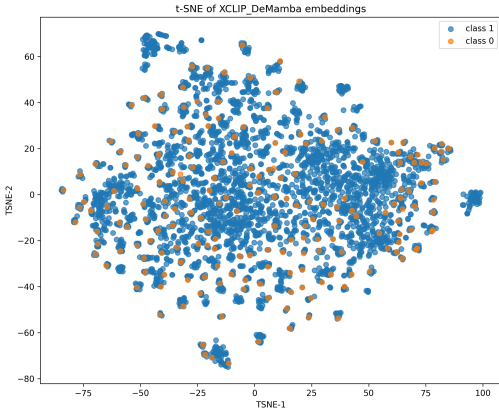


Figure 8. The T-SNE result of Demamba.

rent video generators in maintaining rigid-body constraints during dynamic scenes. *Interaction Inconsistency* (10.0%) and the remaining categories (44.7%) further demonstrate that Skyra attends to diverse physical violations spanning object permanence, causality, and commonsense.

The relatively low proportion of *Low-Level Forgery* (17.2%) suggests that Skyra does not overfit to superficial texture or color cues, which tend to be generator-specific and less generalizable. Instead, its reliance on semantic-level violations aligns with how humans identify AI-generated content, contributing to its stronger cross-generator and cross-dataset generalization observed in Table 6.

Table 7. Distribution of artifacts detected by Skyra on ViF-Bench, organized by our hierarchical taxonomy.

L1 Category (Ratio)	L2 Category (Ratio)	L3 Category	Ratio
Low-Level Forgery (17.2%)	Texture Anomaly (11.2%)	Texture Jittering	3.1%
		Structure Anomaly	3.5%
	Others (6.0%)	Others	4.6%
	
Violation of Laws (82.8%)	Object Inconsistency (28.1%)	Shape Distortion	15.2%
		Abnormal Object Appearance	5.8%
		Others	7.1%
	
	Interaction Inconsistency (10.0%)	Abnormal Multi-Object Merging	2.7%
		General Interaction Anomaly	3.2%
		Others	4.1%
	
Others (44.7%)	

D. Analysis of Detection Capabilities

D.1. Binary Detectors

We take Demamba [5] and NSG-VD [84] as examples of underperforming classifiers that exhibit a strong tendency to label samples as fake.

Demamba: Through T-SNE visualization (Figure 8) and CAM heatmap analysis (Figure 9), we observe that in the T-SNE embedding space, fake and real samples are highly overlapping and difficult to separate. CAM heatmaps further reveal that, for real-labeled videos, the model consistently focuses on similar spatial locations across different samples,

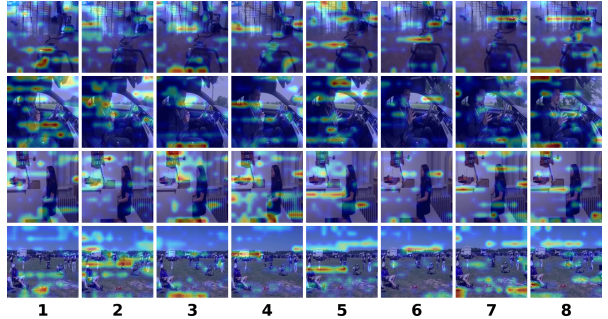


Figure 9. Visualization of Class Activation Maps (CAMs) produced by DeMamba on real video samples.

particularly in the third and fourth frames of the sequences. This suggests that the model may be overly sensitive to fixed visual patterns or preferred spatial locations in the scene, rather than learning generalized content-based cues such as human motion or manipulation traces. Overall, the model does not attend to regions that are discriminative for authenticity, but rather to textures outside the main content of the frame, indicating limited generalization.

NSG-VD: This classifier leverages a reference dataset, providing NSG feature baselines from real videos during inference. Specifically, the normalized spatiotemporal gradient (NSG) features of the reference data are used to model the distribution of real video dynamics, and the maximum mean discrepancy (MMD) between test videos and this reference distribution is computed. A test video is classified as AI-generated if its MMD exceeds a predefined threshold.

In our reproduction, the model achieved near-perfect AU-ROC on the validation set but behaved poorly on the test set, indicating a strong tendency to overfit. This overfitting may stem from the intrinsic sensitivity of NSG-based methods to subtle distributional shifts: the model struggles to generalize when the spatiotemporal dynamics of real videos deviate even slightly from those observed during training. When evaluating NSG-VD on the OOD GenVideo Benchmark, we consider it inappropriate to use the real samples within the GenVideo Benchmark as the reference dataset. Doing so would contradict the purpose of forgery detection and could introduce data leakage. Therefore, we retain the same reference dataset used during training. Similarly, in our robustness study, we do not use real samples under various degraded formats as reference data, because assuming access to degradation-specific real videos for each testing condition is impractical in real-world applications. This decision to reuse the training-time reference dataset may partly explain the suboptimal performance of NSG-VD in both experiments.

Overall, while the reference-dataset mechanism in NSG-VD provides strong detection capability when the distribution of the target data is known or partially accessible, its reliance on such reference information limits its effectiveness in OOD or noisy scenarios, where the real samples to

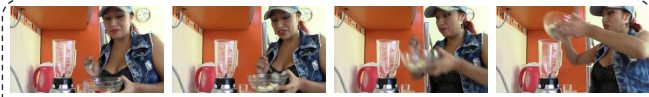


Artifacts Type: Abnormal Human Body Structure

GPT-4.1-mini

<think>The video frames depict a scene at an outdoor event with two men prominently in the foreground, one wearing a white shirt and hat and the other in a black shirt. The background shows a crowd, flags, and vehicles, including a police car. The sequence shows the two men interacting, with the man in white seemingly moving his arm toward the man in black. Step-by-step analysis: 1. From T=0.00s to T=1.31s, the man in white is holding a sign and then begins to move his arm. The motion blur on the man in white's arm and face is quite strong, especially at T=1.00s and T=1.31s, which is consistent with fast movement captured by a camera. This blur looks natural and typical of motion blur in real videos. 2. From T=1.62s to T=2.31s, the man in white's arm moves closer to the man in black, and the motion blur continues. **The interaction between the two men appears fluid, with no sudden jumps or unnatural transitions in their positions or arm movements.** 3. From T=2.62s to T=3.62s, the man in black turns his head toward the man in white, and the man in white's arm is near the man in black's chest. The motion blur on the man in white's arm and the slight blur on the man in black's face are consistent with natural movement and camera capture. 4. From T=4.00s to T=5.00s, the man in white is no longer in the frame, and the man in black is looking to his left. The background remains consistent, with no sudden changes in lighting or object appearance. 5. Throughout the sequence, the lighting on the two men and the background is consistent with a sunny outdoor environment. Shadows and highlights correspond well with the apparent sun position. 6. No signs of texture anomalies, unnatural blurring beyond expected motion blur, or lighting inconsistencies are observed. 7. **The interaction between the two men, including their relative positions and movements, appears physically plausible and continuous.** 8. No abnormal object appearances or disappearances are detected. The police car and background elements remain consistent. 9. The motion blur and slight focus changes are typical of real handheld or moving camera footage. Based on the above observations, there are no detectable artifacts or inconsistencies that would suggest manipulation or forgery. No artifacts to tag.</think>
<answer>Real</answer>

(a) False Negative on Fake Videos



Real Video

Gemini-2.5-flash

<think>The video frames show a woman in a kitchen, wearing a denim vest and a cap, preparing ingredients in a bowl and then attempting to pour them into a blender. Here's a step-by-step analysis:
1. **Initial Observation (T=0.00s - T=4.62s):** The woman is holding a clear glass bowl with chopped ingredients and a spoon, stirring them. A blender is on the counter to her left. The movements appear natural, and the lighting and textures seem consistent.
2. **Action Analysis (T=4.62s):** The woman begins to lift the bowl, preparing to pour its contents into the blender. Her right hand is holding the bottom of the bowl, and her left hand is holding the side.
3. **Critical Frame Analysis (T=5.00s):** At T=5.00s, the woman has lifted the bowl and is tilting it towards the blender. **However, a significant anomaly is observed.** The contents of the bowl, which were clearly visible as chopped ingredients (fruits/vegetables) in previous frames, are now completely gone. **The bowl is empty, yet her hands are positioned as if she is pouring something.** This is a clear **Abnormal Object Disappearance** in <[4.62s, 5.00s]> at <[600, 400, 800, 600]> (referring to the contents of the bowl). The bowl itself is still present, but its contents have vanished.
4. **Further Examination of T=5.00s:** The woman's facial expression and body posture suggest she is actively pouring, but the bowl is empty. This creates a **Violation of General Causality Law** in <[5.00s, 5.00s]> at <[0, 0, 1000, 1000]> as the action of pouring implies contents, which are absent.
Based on the sudden and complete disappearance of the bowl's contents while the pouring action is being performed, the video exhibits a clear manipulation.</think>
<answer>Fake</answer>

(b) False Positive on Real Videos

Figure 10. Response examples of off-the-shelf MLLMs.

be evaluated are either unavailable or should not be incorporated into the reference set in the first place.

D.2. Off-the-Shelf MLLMs

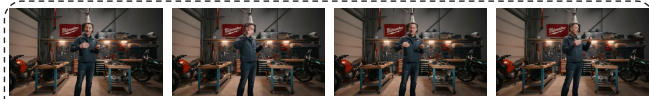
Figure 10 provides concrete examples of the failure modes discussed in the main paper when directly prompting off-the-shelf MLLMs for AI-generated video detection. In panel (a), we show *false negatives* on fake videos. Even with explicit chain-of-thought instructions, most models focus on high-level semantics and overall visual appeal (e.g., “the scene looks natural” or “the movements are smooth”) while overlooking intrinsic forgery cues such as inconsistent geometry or physics-violating motion. As a result, they confidently classify clearly synthetic videos as real and provide rationales that largely describe the content instead of analyzing subtle spatiotemporal artifacts.

Panel (b) shows the opposite pattern. Models such as Gemini-2.5-flash [11] tend to over-interpret natural video degradations, including compression artifacts, motion blur, and low-light noise, as evidence of forgery. In these cases, the model produces detailed yet incorrect explanations that attribute the degradations to “AI generation” rather than common acquisition or post-processing effects. This confirms our quantitative findings that off-the-shelf MLLMs tend to conflate quality with authenticity: they are sensitive to superficial visual cues but struggle to distinguish genuine forgery artifacts from benign imperfections in real-world videos.

D.3. Existing MLLM-based Detectors

We further analyze BusterX++ [72, 73], a recent MLLM-based detector that adapts pretrained models for AIGC video detection. Figure 11 (a) shows a *success case* where BusterX++ correctly identifies an AI-generated video. In such scenarios, the synthetic content exhibits obvious stylistic or aesthetic discrepancies from typical real videos (e.g., overly smooth textures or globally inconsistent lighting), which align well with the model’s training biases and allow it to reach the correct decision.

However, panels (b) highlight the limitations of relying primarily on global scene appearance. Here, the AI-generated clip contains subtle but critical physics-violating artifacts, which humans readily notice. BusterX++, however, focuses on the overall coherence and visual quality of the scene and fails to attend to these localized spatiotemporal inconsistencies, leading to an incorrect “real” prediction. Together, these examples corroborate our main observation that current MLLM-based detectors behave more like general content describers: they emphasize superficial, distribution-level cues and natural degradations, but are not yet equipped to systematically discover and reason about intrinsic forgery artifacts that are crucial for reliable AI-generated video detection.



<think>\nLet's analyze this video step by step to determine if it is real or fake:\n\n1. **Environment and Setting**: The setting appears to be a well-organized workshop or garage, which is typical for a professional or hobbyist working on motorcycles or mechanical projects. The presence of tools, workbenches, and a Milwaukee sign on the wall suggests a professional or branded environment, which is common in real-life settings but can also be staged for a video production.\n\n2. **Lighting and Shadows**: The lighting is consistent and well-distributed, which is characteristic of a controlled environment used in video production. There are no natural light sources that would suggest this is a real-life setting. The shadows and highlights are uniform, indicating the use of professional lighting equipment, which is not typically found in a real garage setting.\n\n3. **Person's Appearance and Movement**: The individual in the video is dressed in a way that suggests a professional or instructional role, possibly a presenter or instructor. The movement and gestures are smooth and practiced, which is typical of a pre-recorded video rather than a live-action scene. The person's attire and the way they are positioned and moving suggest a staged setup rather than a real-life scenario.\n\n4. **Background Elements**: The background includes motorcycles, which are part of the setting, but the overall arrangement and the way they are displayed suggest a controlled environment. The motorcycles are positioned in a way that is typical for a promotional or instructional video, rather than a real-life garage where they would be more casually placed.\n\n5. **Consistency and Quality**: The video quality is high, with no visible grain or noise that one would expect from a real-life recording. The colors are vibrant and the image is sharp, which is indicative of post-production editing and high-quality video production techniques. This level of quality is not typically achieved in real-life recordings.\n\n6. **Contextual Clues**: There are no contextual clues that would suggest this is a real-life scenario. The overall production value, including the lighting, editing, and the controlled environment, points towards a professional video production rather than a real-life recording.\n\nGiven this analysis, it is clear that there are numerous inconsistencies and signs of forgery that indicate this video is not real but rather a fake, likely created for promotional or instructional purposes.\n\nTherefore, the conclusion is that this video is fake.\n\nThe answer is: **B) fake**\n</think>\n\n<answer>**B**</answer>

(a) Success Cases



Artifacts Type: Structure Anomaly

<think>\nLet's analyze this video step by step to determine if it is real or fake:\n\n1. **Scenery and Architecture**: The video shows a modern cityscape with tall skyscrapers, which appear to be real buildings. The architecture is consistent with many urban centers around the world, featuring glass facades and steel structures. **There are no visible signs of digital manipulation or inconsistencies that would suggest a fake environment.**\n\n2. **Water and Reflections**: The water in the foreground reflects the buildings and the sky, which is a common natural phenomenon. The reflections are clear and realistic, showing the typical behavior of water surfaces under sunlight. **There are no artifacts or distortions that would indicate digital alteration.**\n\n3. **Cruise Ship**: The cruise ship is a real vessel, identifiable by its size, design, and the text on its side, which appears to be a real name or branding. The ship is docked at a pier, which is a common sight in many ports around the world. There are no elements that suggest the ship is a digital creation or a model.\n\n4. **Sky and Weather**: The sky is clear with a few clouds, which is a typical weather condition in many cities. The lighting and shadows are consistent with natural sunlight, further supporting the idea that this is a real recording.\n\n5. **Vegetation**: The greenery along the waterfront is lush and appears to be real plants. There are no signs of artificial lighting or unusual growth patterns that would be indicative of a fake video.\n\n6. **Overall Consistency**: There are no elements in the video that suggest it is a forgery. The composition, lighting, and details are all consistent with a real-world scenario. The absence of any digital artifacts or anomalies points to the video being a genuine recording.\n\nGiven this analysis, it is clear that there are no inconsistencies or signs of forgery. The video depicts a real scene of a cruise ship docked in a modern city, likely a port city with a waterfront.\n\nTherefore, **the conclusion is that this video is real.**\n\nThe answer is: **A) real**\n</think>\n\n<answer>**A**</answer>

(b) Failed Cases

Figure 11. Response examples of existing MLLM-based detector, BusterX++ [73].

E. Additional Examples

E.1. Design of Prompts

We specify the system and user prompt that Skyra uses in Figure 12. The system prompt specifies the model's role as an AI video analyst, clearly defines the output format (a <think> reasoning block followed by a one-word <answer> verdict), and constrains the reasoning to our artifact taxonomy, requiring that all findings be tagged with explicit categories, time spans, and bounding boxes. In contrast, the user prompt focuses on supplying multimodal evidence: we interleave sampled frames with their timestamps (e.g., "[T=0.00s] <image>" ... "[T=5.00s] <image>"), so that the model can reason over the evolution of the scene, align artifacts with precise temporal positions, and improve its ability to detect subtle, time-dependent inconsistencies.

E.2. Examples of the Responses of Skyra

We provide the inference examples of Skyra on more samples in ViF-Bench. Figures 16 and 15 demonstrate its responses when encountering real videos. Figure 18- 25 exhibit different types of evidence that Skyra uses when determining that a video is AI-generated.

F. Broader Impacts

Our work is motivated by the growing societal risks posed by AI-generated videos, including large-scale misinformation,

System Prompt:

You are an expert AI video analyst. Your primary task is to review a sequence of video frames and provide a step-by-step analysis of their authenticity.

You MUST output your entire analysis using the following structure:

1. A <think>...</think> block containing your detailed reasoning.
2. An <answer>...</answer> block containing the final, one-word verdict: 'Fake' or 'Real'.

Inside the <think> block, you MUST:

1. Start by briefly describing the overall content of the video frames.
2. Follow a detailed, step-by-step "discovery" or "verification" process.
3. When you identify an artifact (or clear a region), you MUST use a valid L3 Category Name from the "Artifact Category Definitions" provided below.
4. You MUST embed your finding using the following exact tag structure:
<type>L3 Category Name</type> in <time>[startTime, endTime]</time> at <bbox>[x1, y1, x2, y2]</bbox>
5. If multiple artifacts are present, you must find and tag all of them in temporal order.
6. Your entire reasoning process must be self-contained

...
Artifact Category Definitions (Valid L3 Categories for the <type> tag)
...

[Artifact Taxonomy Here]

User Prompt:

Here are the video frames and their corresponding timestamps:

[T=0.00s] <image>
...
[T=4.67s] <image>
[T=5.00s] <image>

Please analyze the video frames, determine if the video is real or fake, and provide your reasoning

Figure 12. System prompt and user prompt design.

impersonation, and erosion of trust in authentic media. By focusing on interpretable, artifact-centric detection, Skyra aims to provide not only predictions but also grounded visual evidence that can assist journalists, fact-checkers, regulators,

Table 8. License of source datasets in ViF-CoT-4K and ViF-Bench.

Dataset	License
Kinetics-400 [29]	CC BY 4.0
Panda-70M [6]	Snap Inc. Non-Commercial Research
HD-VILA-100M [78]	AGPL-3.0

and platform moderators in assessing the authenticity of suspicious content. The ViF-CoT-4K dataset and ViF-Bench further offer a standardized testbed for evaluating new detectors on diverse, up-to-date generators, which may contribute to more reliable and transparent AIGC safety tools.

At the same time, releasing a detailed artifact taxonomy, benchmark, and detector introduces dual-use concerns. In principle, insights into the failure modes of current detectors could inform future attempts to design more robust and evasive generative models. We believe that, on balance, the benefits of enabling the research community, civil society, and industry to build stronger and more interpretable defenses outweigh these risks. To mitigate potential misuse, our datasets contain only curated, non-sensitive content, and we emphasize that Skyra is intended to support human-in-the-loop verification rather than fully automated decision making or mass surveillance. We encourage downstream users to deploy our models and data in accordance with relevant regulations, to combine them with complementary safeguards such as provenance and watermarking, and to continuously stress-test detectors as the landscape of generative video models evolves.

G. License

ViF-CoT-4K and ViF-Bench are provided to the community under CC BY 4.0 license. By downloading our dataset from our website or other sources, the user agrees to adhere to the terms of CC BY 4.0 and the licenses of the source datasets. Licenses of the source datasets are listed in the Table 8.

You are an expert AI video analyst. Your task is to generate meticulous, step-by-step Chain-of-Thought (CoT) reasoning for training a deep learning model. You will be given a set of FAKE video frames, a set of corresponding REAL video frames, and a ground-truth JSON annotation.

Your goal is to generate *two independent annotations* based on this data.

1. Input You Will Receive

1. **[FAKE VIDEO FRAMES]**: 16 sampled frames from the fake video.
2. **[REAL VIDEO FRAMES]**: 16 sampled frames from the real video.
3. **[HUMAN ANNOTATION]**: A JSON object (with Chinese descriptions) that you must use as a reference for *what* to find (in the fake) or *what to clear* (in the real).

2. Output You MUST Generate

You must output *only* a single, valid JSON object with two keys: "fake_cot_annotation" and "real_cot_annotation".

```

...json
{
  "fake_cot_annotation": "...",
  "real_cot_annotation": "...",
}
...

```

3. Rules for "fake_cot_annotation"

The string must follow this structure:

```

<think>...thinking process...</think>\n<answer>Fake</answer>

```

The thinking process **MUST**:

1. Be **fully self-contained**. It must **ONLY** analyze the **[FAKE VIDEO FRAMES]**. Do NOT mention or allude to a real video.
2. Start by describing the video content, then actively scan for artifacts (e.g., "I'm checking the lighting...", "The background texture...").
3. **You MUST** find and integrate ALL pieces of evidence from the [HUMAN ANNOTATION] JSON in **temporal order** as a natural part of your discovery narrative (e.g., "First, I noticed...", "Then, as I kept watching...").
4. For each piece of evidence, embed its tags: <type>L3 Category Name</type> in <[start, end]> at <[x1, y1, x2, y2]>.
5. Your reasoning must be in English. **Do NOT** repeat or quote the Chinese description. Use the Chinese text to **understand** what artifact to look for, then describe that artifact in your **own** English words.

4. Rules for "real_cot_annotation"

The string must follow this structure:

```

<think>...thinking process...</think>\n<answer>Real</answer>

```

The thinking process **MUST**:

1. Be **fully self-contained**. It must **ONLY** analyze the **[REAL VIDEO FRAMES]**. Do **NOT** mention "fake video," "counterpart," "hotspot," or any other data outside of the real frames.
2. Follow a "diligent inspection" narrative. Start by describing the video, then state you are conducting a thorough review for common generation artifacts.
3. **You MUST** proactively inspect and clear ALL regions corresponding to the [HUMAN ANNOTATION] evidence, in temporal order.
4. For each region inspected, reference the tags to specify **what** you are clearing: "...I am checking the area <[start, end]> at <[x1, y1, x2, y2]>."
5. After checking each tagged region, state in your **own** English words that it is clear (e.g., "the text here is stable," "the motion is fluid," "the objects interact correctly").
6. Conclude that the video is real.

5. Artifact Category Definitions

6. Examples (In-Context Learning)

Example 1 (Single Clue + Independent CoT)

[HUMAN ANNOTATION]:

```

...json
{
  "video_id": "b03HGh02Ak-2",
  "evidence": [
    {
      "fake": {
        "category": { "L1": "Violation of Laws", "L2": "Violation of Commonsense", "L3": "Text Distortion" },
        "description": "...",
        "temporal": { "start": 0.91, "end": 5.04 },
        "spatial": [ 0.4, 0.2, 0.6, 0.2 ]
      }
    }
  ]
}
...

```

YOUR REQUIRED OUTPUT:

```

...json
{
  "fake_cot_annotation": "<think>The video appears to be a news report with an anchor and on-screen graphics. I'm scanning the overall scene first. The anchor's face and movement seem stable, no obvious Shape Distortion. The lighting is consistent. My attention is drawn to the on-screen graphics. The main title graphic is sharp, but as I look closer at the text *below* the main title, something is wrong. The characters look like they are flickering and warping. Yes, upon inspection, this is a clear artifact. I see <type>Text Distortion</type> in <[0.91, 5.04]> at <[0.4, 0.2, 0.6, 0.2]> where the text is warped and has no clear semantic meaning.</think>\n<answer>Fake</answer>".
  "real_cot_annotation": "<think>I am analyzing this news report. I will conduct a thorough inspection for any signs of AI generation. The anchor's face and movement appear natural. The lighting is consistent. I am paying close attention to the on-screen text, as this is a common failure point. Specifically, I am examining the lower text area <[0.91, 5.04]> at <[0.4, 0.2, 0.6, 0.2]>. In these frames, the text is perfectly sharp, stable, and legible. It shows no signs of distortion. My review of this clip finds no artifacts.</think>\n<answer>Real</answer>".
}
...

```

Example 2 (Multiple Clues + Independent CoT)

[HUMAN ANNOTATION]:

```

...json
{
  "video_id": "2xgtqmQA0xg-0",
  "evidence": [
    { "fake": { "category": { "L3": "Shape Distortion" }, "temporal": { "start": 0, "end": 0.24 }, "spatial": [ 0.3, 0.6, 0.4, 0.8 ] } },
    { "fake": { "category": { "L3": "Abnormal Multi-Object Merging" }, "temporal": { "start": 0.79, "end": 1.22 }, "spatial": [ 0.1, 0.3, 0.3, 0.6 ] } },
    { "fake": { "category": { "L3": "General Object Identity Inconsistency" }, "temporal": { "start": 3.3, "end": 3.61 }, "spatial": [ 0.3, 0.4, 0.4, 0.6 ] } }
  ]
}
...

```

YOUR REQUIRED OUTPUT:

```

...json
{
  "fake_cot_annotation": "<think>This video shows a close-up of someone assembling small mechanical parts. I am observing the interaction between the hands and the components. The camera is steady. I'll watch the process chronologically. Right at the beginning, I'm focusing on the part in the lower-middle frame. Its shape seems... unstable. It's warping and deforming, which isn't right for a solid part. This is a clear <type>Shape Distortion</type> in <[0, 0.24]> at <[0.3, 0.6, 0.4, 0.8]>. I'll continue watching. Now, around the 1-second mark, the person is picking up another part. As the handheld part touches the fixed part, they... blend together? It looks like the two distinct objects are merging unnaturally. This is a <type>Abnormal Multi-Object Merging</type> in <[0.79, 1.22]> at <[0.1, 0.3, 0.3, 0.6]>. This is very suspicious. Let me keep watching. Later, around 3.3 seconds, my attention is drawn to the part in the person's hand. It was clearly gold-colored a moment ago, but suddenly it flashes and changes to black and silver, with no external cause. This is a <type>General Object Identity Inconsistency</type> in <[3.3, 3.61]> at <[0.3, 0.4, 0.4, 0.6]>. The video has multiple, severe artifacts.</think>\n<answer>Fake</answer>".
  "real_cot_annotation": "<think>I am carefully reviewing this assembly footage to verify its authenticity. I will check several key moments for common artifacts. First, I am checking the component at the start, in area <[0, 0.24]> at <[0.3, 0.6, 0.4, 0.8]>. The part is perfectly rigid and stable; its shape does not change. Next, I'm checking the part interaction around 1 second, in area <[0.79, 1.22]> at <[0.1, 0.3, 0.3, 0.6]>. The handheld part makes contact with the fixed part, but they remain distinct objects. The interaction is normal. Finally, I'm checking the object identity around 3.3 seconds, in area <[3.3, 3.61]> at <[0.3, 0.4, 0.4, 0.6]>. The part in the hand remains a consistent gold color throughout the clip. It does not change. This video passes all checks.</think>\n<answer>Real</answer>".
}
...

```

Figure 13. Chain-of-Thought Annotation Prompt.

Table 9. Hierarchical distribution of artifact categories (L1–L2–L3) in ViF-CoT-4K.

L1 Category	Ratio	L2 Category	Ratio	L3 Category	Ratio
Low-Level Forgery	17.2%	Texture Anomaly	11.2%	Structure Anomaly	3.5%
				Texture Jittering	3.1%
				Unnatural Blur	3.6%
		Color & Lighting Anomaly	5.4%	Color Over-Saturation	2.8%
				Lighting Inconsistency	2.5%
		Move Forgery	1.6%	Camera Motion Inconsistency	1.6%
Violation of Laws	82.8%	Object Inconsistency	28.1%	Abnormal Object Disappearance	3.6%
				Abnormal Object Appearance	5.8%
				Person Identity Inconsistency	1.1%
				General Object Identity Inconsistency	2.4%
				Shape Distortion	15.2%
		Interaction Inconsistency	10.0%	Abnormal Rigid-Body Crossing	2.7%
				Abnormal Multi-Object Merging	2.7%
				Abnormal Object Splitting	1.4%
				General Interaction Anomaly	3.2%
		Unnatural Movement	10.0%	Unnatural Human Movement	6.6%
				Unnatural Animal Movement	0.5%
				Unnatural General Object Movement	2.9%
		Violation of Causality Law	6.90%	Violation of Physical Law	4.1%
				Violation of General Causality Law	2.8%
		Violation of Commonsense	27.8%	Abnormal Human Body Structure	10.5%
Abnormal General Object Structure	3.2%				
Text Distortion	14.1%				

Table 10. Overview of video generation models used to synthesize forged samples in our dataset. “Ref. Cond.” denotes the typical conditioning modes (T2V: text-to-video, I2V: image-to-video, TI2V: text+image-to-video). For commercial closed-source systems, parameter sizes are not publicly disclosed and thus marked as “N/A (closed)”.

Model Name	Release Date	Parameter	Ref. Cond.	Inference	Sample Number	HyperLink
Wan2.1-1.3B-T	2025-02-25	1.3B	T2V	Local	750	Link
CogVideoX1.5-T	2024-08	5B	T2V	Local	744	Link
CogVideoX1.5-I	2024-08	5B	I2V	Local	760	Link
Wan2.2-TI2V-5B(T2V)	2025-08-28	5B (MoE)	T2V	Local	747	Link
Wan2.2-TI2V-5B(I2V)	2025-08-28	5B (MoE)	I2V	Local	748	Link
HunyuanVideo	2024-12-03	13B	T2V	Local	750	Link
HunyuanVideo-I2V	2025-05-06	13B	I2V	Local	968	Link
VACE-1.3B-T (Wan2.1-VACE-1.3B)	2025-05-14	1.3B	T2V	Local	165	Link
Wan2.2-T2V-A14B	2025-08-28	14B (MoE)	T2V	Local	165	Link
Wan2.2-I2V-A14B	2025-08-28	14B (MoE)	I2V	Local	165	Link
SkyReels-V2-T2V	2025-04-21	14B	T2V	Local	165	Link
SkyReels-V2-I2V	2025-04-21	14B	I2V	Local	164	Link
LTX-Video(T2V)	2025-05-06	13B	T2V	Local	165	Link
LTX-Video(I2V)	2025-05-06	13B	I2V	Local	165	Link
Gen4-Turbo	2025-04	N/A (closed)	I2V	API	121	Link
Hailuo-02	2025-06-18	N/A (closed)	T2V	API	137	Link
Pika-V2	2025-08-15	N/A (closed)	T2V	API	151	Link
Pixverse-V4-5	2025-05	N/A (closed)	T2V	API	152	Link
Kling-V1	2024-06	N/A (closed)	T2V	API	141	Link
Sora-2	2024-02-15	N/A (closed)	T2V	API	150	Link

Note. Dates are approximate and refer to the first public announcement or open release of the corresponding model family. For commercial systems with undisclosed architecture/size, “Parameter” is marked as “N/A (closed)”.

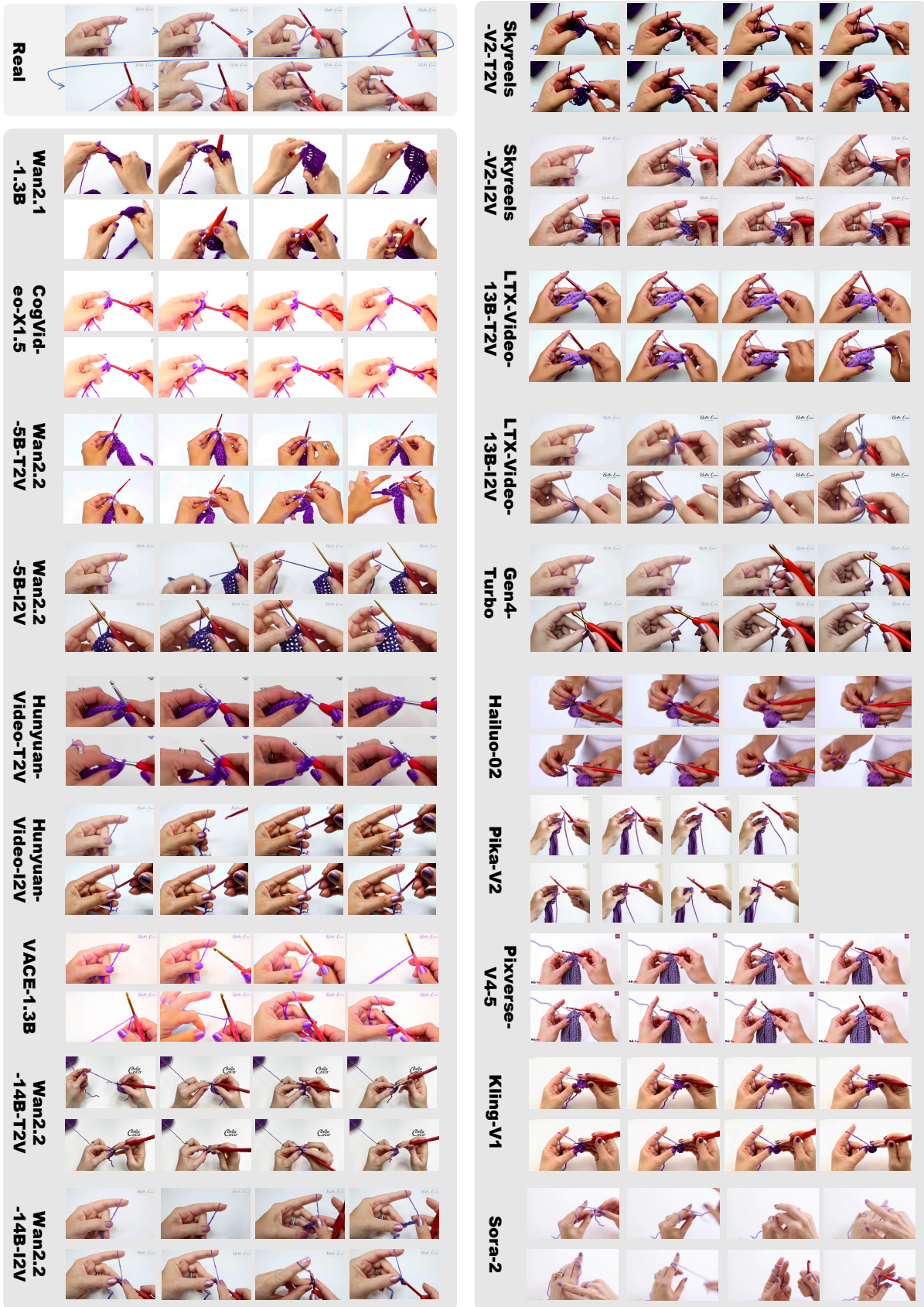


Figure 14. ViF-Bench Video Sample Examples-I

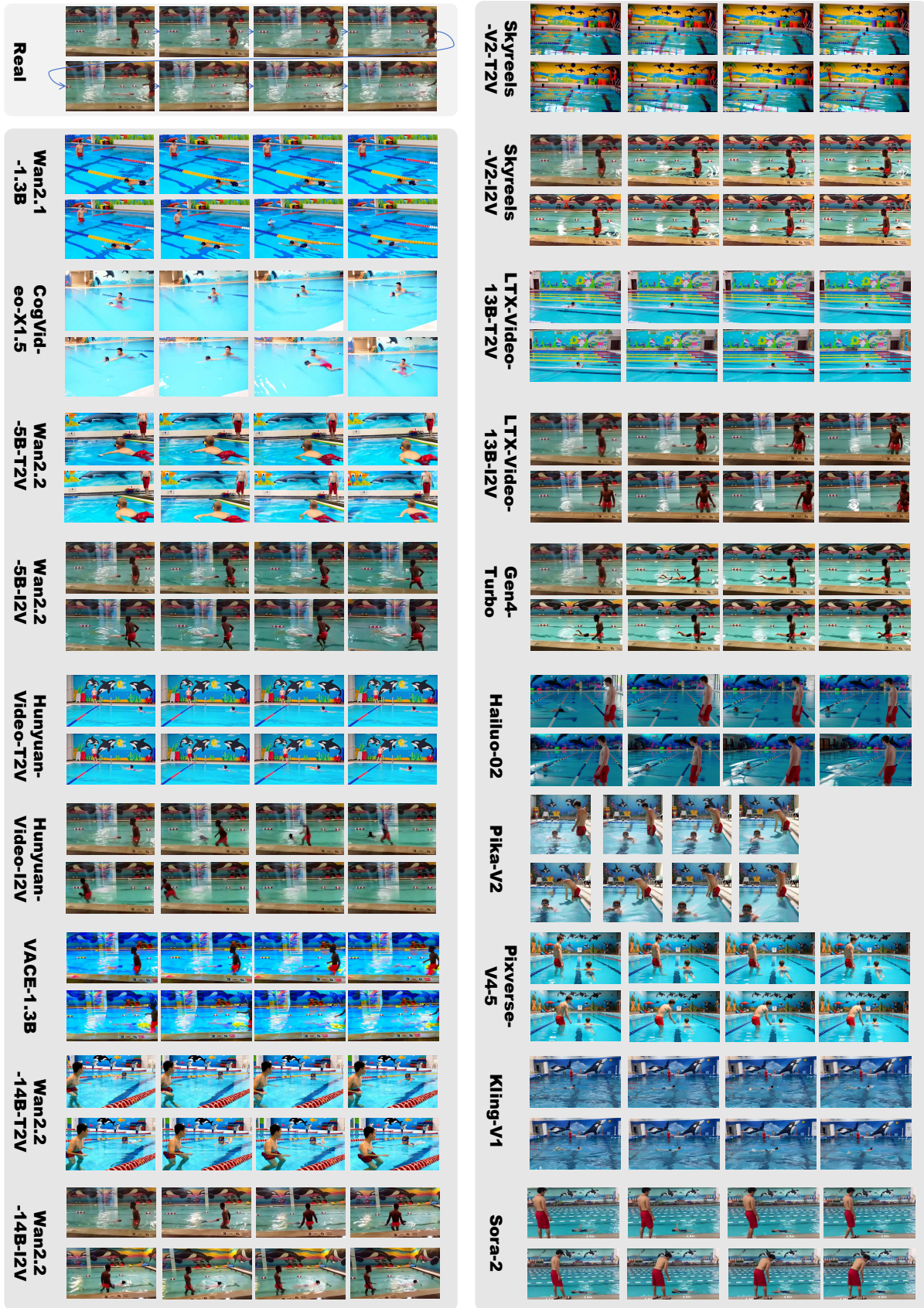


Figure 15. ViF-Bench Video Sample Examples-II

System Prompt: You're an ...Your primary task is to review a sequence of video frames and provide a step-by-step analysis of their authenticity.
User Prompt: Here are the video frames... Please analyze the video frames, determine if the video is **real** or **fake**, and provide your reasoning



Skyra

<think>I am conducting a thorough analysis of this video, which shows a person preparing a pasta casserole in a glass dish. I will meticulously check for any signs of digital manipulation or generation artifacts. First, I am examining the initial action of the person placing a wooden spoon into the dish, specifically in the area $\langle t \rangle [0.0, 0.55] \langle /t \rangle$ at $\langle bbox \rangle [0.3, 0.2, 0.8, 0.6] \langle /bbox \rangle$. The spoon is held by the person and is clearly inserted by them into the pasta. The interaction is physically plausible and natural. Next, I am inspecting the movement of the spoon as it stirs the pasta, focusing on the region $\langle t \rangle [0.9, 1.55] \langle /t \rangle$ at $\langle bbox \rangle [0.3, 0.2, 0.8, 0.5] \langle /bbox \rangle$. The spoon moves fluidly and remains a solid, rigid object throughout the motion. There is no evidence of warping, bending, or any form of distortion. Finally, I am observing the person's hand from the side, in the area $\langle t \rangle [2.4, 3.06] \langle /t \rangle$ at $\langle bbox \rangle [0.1, 0.0, 0.4, 0.4] \langle /bbox \rangle$, to check for any anatomical inconsistencies. The hand and fingers maintain a normal, consistent shape and structure as they guide the spoon. After a detailed inspection, I find no artifacts or violations of physical laws. The video appears to be authentic.</think>
 <answer>Real</answer>

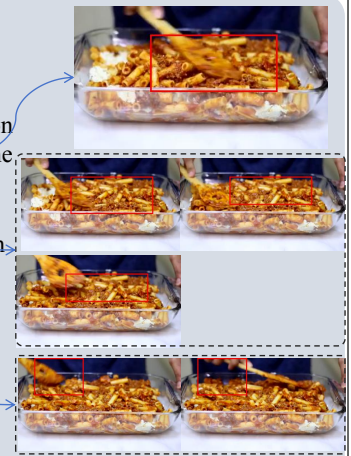


Figure 16. Skyra's Response Example on Real Videos, I

System Prompt: You're an ...Your primary task is to review a sequence of video frames and provide a step-by-step analysis of their authenticity.
User Prompt: Here are the video frames... Please analyze the video frames, determine if the video is **real** or **fake**, and provide your reasoning



Skyra

<think>I am analyzing a video of a man with a distinctive white, curly wig speaking into a microphone. My goal is to conduct a thorough inspection to verify its authenticity. I will pay close attention to common areas where digital artifacts might appear, such as detailed textures. I am specifically examining the man's hair, as it is a complex texture that can be difficult to render correctly. I am checking the area $\langle t \rangle [0.0, 5.06] \langle /t \rangle$ at $\langle bbox \rangle [0.3, 0.1, 0.7, 0.8] \langle /bbox \rangle$ throughout the clip. Upon careful review, the hair's texture appears completely natural. I can see the definition of individual strands and curls, and the way light reflects off it is consistent with the environment. There is no unnatural blur, smudging, or static, grain-like noise. The texture is clear and moves realistically as the man speaks and gestures. Having found no evidence of digital manipulation, I conclude the video is authentic.</think>
 <answer>Real</answer>



Figure 17. Skyra's Response Example on Real Videos, II

System Prompt: You're an ...Your primary task is to review a sequence of video frames and provide a step-by-step analysis of their authenticity.
User Prompt: Here are the video frames... Please analyze the video frames, determine if the video is **real** or **fake**, and provide your reasoning



Skyra

<think>The video shows a static shot of a city skyline across a body of water. The scene appears to be a sunny day with some clouds. I will scan the video for any potential artifacts. My attention is first drawn to the water in the foreground. The surface of the water is not calm; there are visible ripples and reflections from the buildings. However, the texture of the water looks unnatural. Instead of a smooth flow or a natural reflection of light, the surface appears grainy and distorted, with a strange, noisy pattern that doesn't match the movement of the water. This is a clear sign of an artifact. I can identify this as <type>**Texture Jittering**</type> in <t>**[0.0, 5.06]**</t> at <bbox>**[0.0, 0.6, 1.0, 1.0]**</bbox>. Next, I'll examine the buildings in the background. I'm focusing on the cluster of buildings in the center of the frame. As I watch the video, I notice that the structure of the buildings is not stable. The windows and walls seem to flicker and change shape slightly throughout the clip. For example, the green skyscraper on the left appears to warp and the windows on the buildings in the middle seem to shift and distort. This is not a natural change in perspective or lighting. This is a <type>**Structure Anomaly**</type> in <t>**[0.0, 5.06]**</t> at <bbox>**[0.3, 0.0, 0.6, 0.5]**</bbox>. The presence of these two distinct artifacts confirms the video is not authentic.</think> <answer>**Fake**</answer>

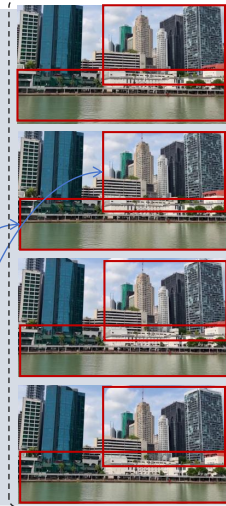


Figure 18. Skyra's Response Example on Fake Videos, Texture Anomaly-Structure Anomaly

System Prompt: You're an ...Your primary task is to review a sequence of video frames and provide a step-by-step analysis of their authenticity.
User Prompt: Here are the video frames... Please analyze the video frames, determine if the video is **real** or **fake**, and provide your reasoning



Skyra

<think>The video shows a wide shot of a park-like setting with many green trees spaced out across a large, manicured lawn. The camera appears to be static. I am examining the overall visual quality of the scene. My attention is immediately drawn to the color of the grass. It looks unnaturally vibrant and uniform, almost like a bright green carpet rather than natural grass. The color is extremely intense and lacks the subtle variations in shade, texture, and shadow that would be present in a real-world scene. This appears to be a consistent issue throughout the entire clip. This is a clear case of <type>**Color Over-Saturation**</type> in <t>**[0.0, 5.06]**</t> at <bbox>**[0.0, 0.5, 1.0, 1.0]**</bbox>, where the grass is excessively and unnaturally colored. The lack of realistic detail and the overly saturated hue strongly suggest the video is not authentic.</think> <answer>**Fake**</answer>



Figure 19. Skyra's Response Example on Fake Videos, Color & Lighting Anomaly-Color Over-Saturation

System Prompt: You're an ...Your primary task is to review a sequence of video frames and provide a step-by-step analysis of their authenticity.
User Prompt: Here are the video frames... Please analyze the video frames, determine if the video is **real** or **fake**, and provide your reasoning



Skyra

<think>The video shows a person from a first-person perspective, driving a red convertible car on a suburban street. The person is wearing a red cap with a Ferrari logo. The car is moving forward, and the camera is positioned inside the vehicle, looking out through the front windshield. I am scanning the video for any visual artifacts. The overall scene appears stable, but I'm paying close attention to the movement of objects. As I watch the video progress, I notice something strange happening in the background. While the car is moving forward, the trees and houses on both sides of the road are not static. They seem to be jittering and shaking in a very unnatural, high-frequency manner. This is not consistent with the smooth motion of a car on a road. This erratic movement is a clear sign of an artifact. I can identify this as <type>Camera Motion Inconsistency</type> in <t>[0.49, 4.85]</t> at <bbox>[0.1, 0.1, 0.9, 0.8]</bbox>, where the background elements exhibit a rapid, jittery vibration that does not match the expected motion of the vehicle. This makes the video feel unstable and generated.</think><answer>Fake</answer>

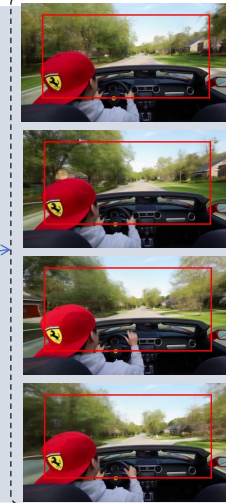


Figure 20. Skyra's Response Example on Fake Videos, Move Forgery-Camera Motion Inconsistency

System Prompt: You're an ...Your primary task is to review a sequence of video frames and provide a step-by-step analysis of their authenticity.
User Prompt: Here are the video frames... Please analyze the video frames, determine if the video is **real** or **fake**, and provide your reasoning



Skyra

<think>The video shows a chef in a professional kitchen, standing behind a counter with various ingredients and bowls laid out. The chef is wearing a traditional white uniform and a tall white hat. He appears to be giving a presentation or a cooking demonstration. Initially, he is gesturing with his hands while speaking. I'm scanning the video for any visual inconsistencies. The background, lighting, and the chef's face seem generally stable. However, as I continue to watch, my attention is drawn to his hands as he moves them. Around the 2.3-second mark, the chef's hands start to look strange. As he gestures, his hands seem to lose their defined structure. They become blurry and appear to warp, with the fingers and palm blending together in an unnatural way. This is not just motion blur; the actual shape of the hands is deforming. This is a clear example of <type>Shape Distortion</type> in <t>[2.34, 3.41]</t> at <bbox>[0.3, 0.3, 0.8, 0.6]</bbox>. The hands repeatedly lose their proper anatomical form as they move, which is a strong indicator of a generated video.</think><answer>Fake</answer>

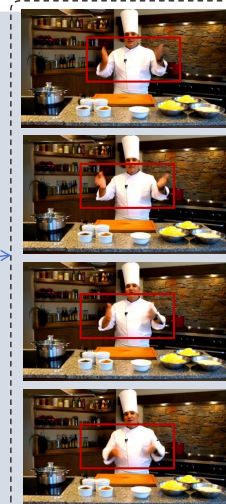


Figure 21. Skyra's Response Example on Fake Videos, Object Inconsistency-Shape Distortion

System Prompt: You're an ...Your primary task is to review a sequence of video frames and provide a step-by-step analysis of their authenticity.
User Prompt: Here are the video frames... Please analyze the video frames, determine if the video is **real** or **fake**, and provide your reasoning



Skyra

<think>The video shows a first-person perspective of a person drinking from a plastic water bottle. The person is wearing a black jacket and glasses. The setting appears to be indoors, with ceiling lights visible. I am analyzing the video for any signs of digital manipulation. The overall scene seems plausible at first glance. I'll focus on the action of drinking. The person brings the bottle to their mouth and takes several sips. As I watch the sequence, I notice something strange happening around the person's mouth area. Starting around the 1.3-second mark, the person's mouth and the bottle's opening seem to blend together in an unnatural way. The boundary between the person's skin, the lips, and the plastic of the bottle becomes indistinct and wobbly. This is not how two solid objects should interact. This is a clear case of **Abnormal Rigid-Body Crossing** in <t>[1.29, 2.41]</t> at <bbox>[0.4, 0.0, 0.6, 0.3]</bbox>, where the person's mouth and the bottle appear to merge and pass through each other as the person drinks. This physical impossibility confirms the video is not authentic.</think>
 <answer>**Fake**</answer>

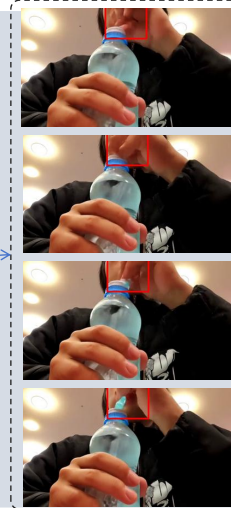


Figure 22. Skyra's Response Example on Fake Videos, Interaction Inconsistency-Abnormal Rigid-Body Crossing

System Prompt: You're an ...Your primary task is to review a sequence of video frames and provide a step-by-step analysis of their authenticity.
User Prompt: Here are the video frames... Please analyze the video frames, determine if the video is **real** or **fake**, and provide your reasoning



Skyra

<think>The video shows a sports team, dressed in green and white uniforms, performing what appears to be a pre-game ritual or huddle on a large, grassy field in front of a massive crowd. I'm analyzing the movements of the players for any inconsistencies. Initially, the players are mostly stationary, facing each other. As the video progresses, there is a lot of motion. However, the movements seem strange and do not follow the rules of physics or common sense. Players on the left side of the frame, particularly the one in the blue jersey, seem to glide and float into position rather than running or jumping. The overall choreography is complex, but the individual player movements are disjointed and don't seem to have a clear, logical purpose. For example, the player in the center wearing number 10 seems to phase through other players or simply appear in different positions without a natural cause. The entire sequence feels like a poorly animated dance rather than a real athletic performance. This is a clear case of **Unnatural Human Movement** in <t>[0.0, 5.06]</t> at <bbox>[0.0, 0.3, 1.0, 0.8]</bbox>, as the players' running, jumping, and interacting motions are illogical and physically impossible.</think><answer>**Fake**</answer>



Figure 23. Skyra's Response Example on Fake Videos, Unnatural Movement-Unnatural Human Movement

System Prompt: You're an ...Your primary task is to review a sequence of video frames and provide a step-by-step analysis of their authenticity.
User Prompt: Here are the video frames... Please analyze the video frames, determine if the video is **real** or **fake**, and provide your reasoning



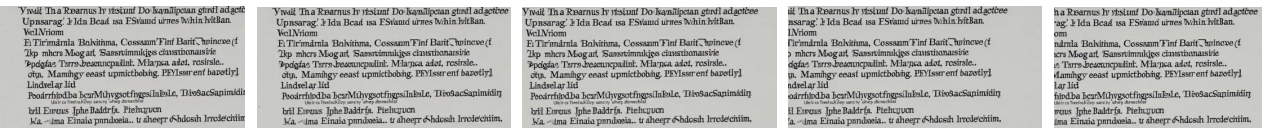
Skyra

<think>The video shows a close-up of a glass mug filled with a yellowish liquid, likely tea, resting on a white wooden surface. A spoon is already in the liquid. I'll watch the sequence of events. The scene is static for the first couple of seconds. Then, starting around the 3-second mark, a stream of liquid is poured into the mug from above. As this new liquid enters the mug, I notice something very strange. The surface of the tea inside the mug ripples and distorts in a way that doesn't seem physically correct. The ripples appear to travel through the liquid and even seem to form and cancel each other out in mid-air, which is impossible. This is a clear **Violation of Physical Law** in **[3.05, 4.35]** at **[0.4, 0.1, 0.7, 0.7]**, as the liquid's behavior defies the physics of fluid dynamics. The way the ripples form and cancel is not how a real liquid would behave when poured into another container.</think>
 <answer>**Fake**</answer>



Figure 24. Skyra's Response Example on Fake Videos, Violation of Causality Law-Violation of Physical Law

System Prompt: You're an ...Your primary task is to review a sequence of video frames and provide a step-by-step analysis of their authenticity.
User Prompt: Here are the video frames... Please analyze the video frames, determine if the video is **real** or **fake**, and provide your reasoning



Skyra

<think>The video displays a static screen filled with lines of text. The characters appear to be a mix of English letters and other symbols, but they form no recognizable words or language. The text is arranged in multiple paragraphs. I am examining the video for any signs of artificial generation. The overall appearance is consistent, with no camera movement. I will now focus on the content of the text. As I scan through the frames, I notice that while the characters within a single line of text seem stable, the lines themselves are not perfectly straight. They exhibit a subtle, high-frequency jitter, as if wobbling or warping slightly. This is particularly noticeable at the beginning of the video. This is a clear sign of an artifact. I have identified **Text Distortion** in **[0.0, 1.27]** at **[0.1, 0.1, 0.9, 0.9]**, where the lines of text are unnaturally bent and unstable. This distortion persists for the first couple of seconds, confirming the artificial nature of the text.</think>
 <answer>**Fake**</answer>

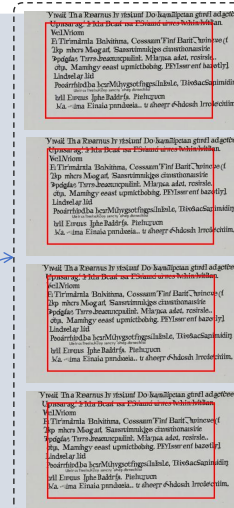


Figure 25. Skyra's Response Example on Fake Videos, Violation of Commonsense-Text Distortion